AWARD NUMBER: W81XWH-22-1-0394

TITLE: Innate Immune Cytosolic DNA Sensors as Novel Protumorigenic Drivers in Stomach Cancer

PRINCIPAL INVESTIGATOR: Brendan Jenkins

CONTRACTING ORGANIZATION: Monash University , Clayton, Victoria, Australia

REPORT DATE: July 2023

TYPE OF REPORT: Annual

PREPARED FOR: U.S. Army Medical Research and Development Command
Fort Detrick, Maryland 21702-5012

REPORT DOCUMENTATION PAGE

Form Approved
OMB No. 0704-0188

1. REPORT DATE	**2. REPORT TYPE**	**3. DATES COVERED**
July 2023	Annual	01Jul2022 to 30Jun2023

4. TITLE AND SUBTITLE

Innate Immune Cytosolic DNA Sensors as Novel Protumorigenic Drivers in Stomach Cancer

5a. CONTRACT NUMBER
W81XWH-22-1-0394

5b. GRANT NUMBER
CA210128

5c. PROGRAM ELEMENT NUMBER

6. AUTHOR(S)

Brendan Jenkins

E-Mail: Brendan.jenkins@hudson.org.au

5d. PROJECT NUMBER

5e. TASK NUMBER

5f. WORK UNIT NUMBER

7. PERFORMING ORGANIZATION NAME(S) AND ADDRESS(ES)

Monash University
Department of Molecular and Translational Sciences
27-31 Wright Street,
Clayton, Victoria
3168 Australia

8. PERFORMING ORGANIZATION REPORT NUMBER

9. SPONSORING / MONITORING AGENCY NAME(S) AND ADDRESS(ES)

U.S. Army Medical Research and Development Command
Fort Detrick, Maryland 21702-5012

10. SPONSOR/MONITOR'S ACRONYM(S)

11. SPONSOR/MONITOR'S REPORT NUMBER(S)

12. DISTRIBUTION / AVAILABILITY STATEMENT

Approved for Public Release; Distribution Unlimited

13. SUPPLEMENTARY NOTES

14. ABSTRACT

Purpose/scope: The majority of gastric cancer (GC) cases is associated with chronic inflammation resulting from uncontrolled activation of the body's two arms of the immune system, innate and adaptive immunity. However, current immune-based treatments for GC patients have only focused on a select few adaptive immune checkpoint inhibitors with limited clinical benefits, whereas the clinical utility of innate immunity remains underexplored in GC. **Major findings:** Using a chronic *Helicobacter felis* infection model of early stage GC, we discovered that the innate immune cytosolic DNA sensor AIM2 plays a key role in driving gastric epithelial and immune cellular proliferation in response to *Helicobacter* infection. Conversely, by modeling for late stage gastric tumorigenesis using human GC patient organoids and cell lines, AIM2 augmented human GC cell migration. **Up-to-date progress:** Aim 1 - major task 1 and 2/subtask 1 completed, major task 2/subtask 2 ongoing, major task 3 yet to begin, major task 4 ongoing. Aim 2 - major task 1 completed, major task 2/subtasks 1 and 3 ongoing, subtask 2 yet to begin. Aim 3 - major tasks 1-3 are yet to begin. **Significance:** Thus far, our findings strongly support a dual role for AIM2 in early and late stages of GC.

15. SUBJECT TERMS

AIM2; cell lines; clinical biopsies and datasets; CRISPR gene targeting; cytosolic DNA sensors; gastric cancer; gastritis; *Helicobacter pylori* infection; organoids; transcriptomics; xenografts.

16. SECURITY CLASSIFICATION OF:			**17. LIMITATION OF ABSTRACT**	**18. NUMBER OF PAGES**	**19a. NAME OF RESPONSIBLE PERSON**
					USAMRDC
a. REPORT	**b. ABSTRACT**	**c. THIS PAGE**			**19b. TELEPHONE NUMBER** *(include area code)*
Unclassified	Unclassified	Unclassified	Unclassified	40	

TABLE OF CONTENTS

1. Introduction

Stomach cancer (gastric cancer; GC) is the third most lethal cancer in the world, and is associated with chronic inflammation triggered by a dysregulated innate immune response to various environmental risk factors, in particular infection with the gastric pathogen *Helicobacter pylori* (*H. pylori*). A common disease-associated consequence of *H. pylori* infection is genotoxicity on gastric epithelial cells, leading to double-strand (ds) DNA breaks within the nucleus of the transformed gastric epithelium that are a hallmark of GC. However, a mechanistic link between cellular DNA damage within the gastric epithelium and dysregulated innate immunity promoting inflammation-associated GC has not been established. Although the identity of innate immune regulators that promote GC is ill-defined, the discovery that specific innate immune pattern recognition receptors (i.e. AIM2, cGAS, DDX41, DHX9, DHX36, PRKDC, IFI16, LRRFIP1, Rad50, STING, XRCC6, ZBP1) are cytosolic sensors of microbial DNA and host DNA (e.g. dsDNA breaks in damaged cells) has opened up a new paradigm on how innate immunity can orchestrate pathophysiological responses. However, the role of cytosolic DNA sensors in the pathogenesis of GC is unknown. Therefore, the primary purpose and scope of our research over this reporting period was to demonstrate the pro-tumorigenic activity of a lead candidate innate immune cytosolic DNA sensor, AIM2, upon its CRISPR/Cas9-mediated genetic targeting in human GC cell lines and organoids, as well as in a mouse model of *Helicobacter*-driven gastric disease.

2. Keywords

Absent-In-Melanoma 2 (AIM2)
Cell lines
CRISPR/Cas9 gene editing
Cytosolic DNA sensors
Expression profiling
Helicobacter infection-driven GC model
Innate immunity
Inflammation
Migration
Organoids
Pattern recognition receptors
Proliferation

3. Accomplishments

Major goals of the project

The overall objective of this project is to reveal specific cytosolic DNA sensors as key drivers of GC, and thus set the stage for their future development as new innate immune-based disease biomarkers (e.g. prognostic, predictive) and therapeutic targets for clinical implementation in GC. To do this, we proposed 3 major aims in our approved “Statement of Work” (SOW), each with sub-aims, to achieve this goal.

Aim 1: To identify pro-tumorigenic innate immune cytosolic DNA sensors by CRISPR/Cas9-mediated genetic screening in preclinical human gastric cancer organoids in vitro and in vivo (xenografts).

Aim 2: To demonstrate in vivo that genetic targeting of specific innate immune cytosolic DNA sensors suppresses Helicobacter-driven gastric pathology.

Aim 3: To discover molecular signatures as biomarkers for the activation of specific innate immune cytosolic DNA sensors in gastric cancer using preclinical models, and patient biopsies and datasets.

As shown in the updated SOW below (see Table), we have made significant progress towards addressing these aims in the first year of the grant. Notably, there have been some changes in the order of the original milestones outlined (see "Updated target month of completion" column in the Table), and the reasons for this are detailed further in section 5 ("Changes/Problems").

Table: Updated SOW, end of month 12

Aim 1: To identify pro-tumorigenic innate immune cytosolic DNA sensors by CRISPR/Cas9-mediated genetic screening in preclinical human gastric cancer organoids *in vitro* and *in vivo* (xenografts).	**Original target month of completion**	**Updated target month of completion**	**Percentage completed**
Major Task 1: ACURO approval.	-1		100%
Major Task 2: Selection and manipulation of PDOs			
Subtask 1: In *Aim 1.1*, screen for high (PDO-T^{Hi}) versus low (PDO-T^{Lo}) expressing tumor PDOs for each human cytosolic DNA sensor (up to n = 3 PDO-T^{Hi} and PDO-T^{Lo} for each) by RNASeq and immunoblotting (IB).	2		100%
Subtask 2: Knock-down or over-express each cytosolic DNA sensor in their corresponding PDO-T^{Hi} or PDO-T^{Lo} organoids, respectively. Also stimulate PDOs with commercially-available agonists for specific cytosolic DNA sensors. Over 96 hours, measure growth (e.g. EdU whole mount immunofluorescence (IF)) and migration (scratch-wound assays) potential, production of inflammatory mediators by ELISA (culture supernatants) and qPCR (RNA), as well as activation of inflammatory signaling pathways by IB. Assess DNA damage (γ-H2AX) by IF and/or IB.	2-4	To be determined (see section 5)	15%
Major Task 3: PDO/immune cell co-cultures with *Helicobacter* infection.			
Subtask 1: In *Aim 1.2*, the above PDO-T series from Major Task 2, Subtask 2, will also be co-cultured with isolated human immune cells (e.g. dendritic cells, cytotoxic T lymphocytes) with and without *H. pylori* infection, the latter induced by microinjection with clinically-relevant *H*. *pylori* strains.	5-6	To be determined (see section 5)	0%
Subtask 2: As per Major Task 2, Subtask 2, growth, migration and inflammatory responses, as well as DNA damage, will be measured at multiple time points over 96 hours.	5-6	To be determined (see section 5)	0%
Major Task 4: *In vivo* growth of naïve and 'humanized' PDXs.	Months		
Subtask 1: In *Aim 1.3*, subcutaneously engraft n = 1 representative naïve parental PDO-T^{Hi} or PDO-T^{Lo} organoid, as well as its corresponding knock-down or over-expressing PDO-T, respectively, for each cytosolic DNA sensor of interest (selected	7-8	To be determined (see section 5)	15%

from *Aims 1.1* and *1.2*; Major Tasks 2 and 3) in immunodeficient NSG mice. For each gene, 4 groups × 8 mice/group = 32 mice.			
Subtask 2: Measure tumor growth (volumes, final weights) of each subcutaneous PDX (Subtask 1), and assess general histopathology and cellular processes by immunohistochemistry (IHC), the latter including proliferation (e.g. Ki67), apoptosis (e.g. active Caspase-3), angiogenesis (CD31) and DNA damage, as well as infiltrating pan immune cells (CD45), distinct immune cell types (e.g. F4/80, Gr-1, B220, CD3), and immune cell activation (e.g. CD40, CD69, CD86). Also, IF will be performed with the above antibodies, including those against pan epithelial cells (e.g. EpCam), distinct gastric epithelial cell types (e.g. H/K ATPase), mesenchymal (Vimentin) and fibroblast (PDGFRα) cells, and selected cytosolic DNA sensors.	8-10	To be determined (see section 5)	15%
Subtask 3: Orthotopic PDX in NSG mice for 1 representative PDO-T^{Hi} and corresponding PDO-T^{Hi} knock-down for each cytosolic DNA sensor (Major Task 4, Subtasks 1 and 2). Measure tumor growth, histopathology and cellular processes as per Major Task 4, Subtask 2. For each gene, 2 groups × 8 mice/group = 16 mice.	10-12	To be determined (see section 5)	0%
Subtask 4: For each cytosolic DNA sensor of interest from the above naïve NSG mouse PDXs (Major Task 4, Subtasks 1 and 3), n = 1 representative subcutaneous and orthotopic PDO-T^{Hi} and corresponding PDO-T^{Hi} knock-down will be IV injected with autologous PBMCs (i.e. human immune cells) at tumor engraftment. Tumor growth, general histopathology and cellular processes of humanized PDXs will be assessed as per Major Task 4, Subtask 2. Confirm reconstitution of human immune cells (e.g. CD45, CD3) in blood and tumor xenografts (flow cytometry, IHC). For each gene, 4 groups × 8 mice/group = 32 mice.	12-15	To be determined (see section 5)	0%
Aim 2: To demonstrate *in vivo* that genetic targeting of specific innate immune cytosolic DNA sensors suppresses *Helicobacter*-driven gastric pathology.	**Original target month of completion**	**Updated target month of completion**	**Percentage completed**
Major Task 1: ACURO approval.	-1		100%
Major Task 2:			
Subtask 1: Wild-type (WT) and knock-out (KO) mouse strains for up to 3 cytosolic DNA sensors (existing; BJJ) and/or newly generated (CRISPR/Cas9 GFP-reporter KO mouse lines; PT) will be gavaged (BJJ) with *H. felis* or control broth. At 2- and 4-months post gavage, whole mouse stomach tissues will be collected for sections to	16-28		33%

assess i) histopathology and gastric mucosal thickness (H&E), ii) cellular processes (i.e. proliferation, apoptosis, angiogenesis, DNA damage, inflammation) by IHC, iii) IF (including antibodies against selected cytosolic DNA sensors or GFP-reporter KO mice) for colocalization with specific cell types and cellular processes in the stomach, and iv) intestinal metaplasia by Alcian blue/PAS staining (all by BJJ). 4 genotypes (3 KO, WT) × 2 gavage groups × 2 time points × 8 mice/group = 128 mice.			
Subtask 2: In a second cohort of gavaged WT and KO mice (Major Task 2, Subtask 1) at 2 and 4 months, flow cytometry on stomach single cell suspensions will be used to analyze gastric inflammatory cell infiltrates. 128 mice.	28-29		0%
Subtask 3: In a third cohort of gavaged WT and KO mice (Major Task 2, Subtask 1) at 2 and 4 months, from snap-frozen stomach tissues measure the expression of cytosolic DNA sensors, inflammatory mediators, and/or activation of oncogenic and inflammatory signaling pathways by qPCR (RNA) and/or ELISA and IB (protein lysates). 128 mice.	28-29		33%
Aim 3: To discover molecular signatures as biomarkers for the activation of specific innate immune cytosolic DNA sensors in gastric cancer using preclinical models, and patient biopsies and datasets.	**Original target month of completion**	**Updated target month of completion**	**Percentage completed**
Major Task 1: RNASeq transcriptome profiling.	Months		
Subtask 1: In *Aim 3.1*, up to 3 selected gene-targeted cytosolic DNA sensors, RNASeq will be performed on bulk stomach tissues from i) a representative gene-deficient and non-targeted control orthotopic naive versus humanized PDX (Aim 1, Major Task 4, Subtasks 3 and 4), and ii) *H. felis* versus broth gavaged gene KO and WT control mice (Aim 2, Major Task 2, Subtask 1). For 3 genes, PDXs (32 mice/gene = 96 mice) + gavage (64 mice) = 160.	28-32		0%
Major Task 2: Functional validation.	Months		
Subtask 1: In *Aim 3.2*, expression of the top 10 (up or down) candidate effector genes for each of the 3 selected cytosolic DNA sensors (*Aim 3.1*) will be validated by qPCR in both gene deficient and over-expressing tumor PDO-Ts.	32		0%
Subtask 2: CRISPR/Cas9 KO or over-expression of each candidate regulated gene in tumor PDO-Ts (from Aim 3, Major Task 2, Subtask 1), as naïve and immune cell co-cultures with/ without *H. pylori* (Aim 1, Major Task 3). As per Aim 1, Major Task 2, Subtask 2, growth, migration and inflammatory responses, as well as DNA damage,	32-34		0%

will be measured.			
Major Task 3: Translational validation.	Months		
Subtask 1: In *Aim 3.3*, in clinical samples and transcriptome datasets, assess correlations between expression of candidate cytosolic DNA sensors and validated target genes (Aim 3, Major Task 2, Subtasks 1 and 2), as well as clinicopathological features (e.g. survival, *H. pylori* status, therapy response).	34-36		0%

Accomplishment under these goals

Aim 1: The major accomplishment for this reporting period for Aim 1 relates to Major Task 2, Subtasks 1 and 2. Here, we screened our series of tumour patient-derived organoids (PDO-Ts) from GC patients for high versus low expression of known innate immune cytosolic DNA sensors (Subtask 1). The RNASeq data in Figure 1A below indicate select PDO-Ts that display high or low expression of representative DNA sensors. In Figure 1B and C, AIM2 knock down by CRISPR (AIM2-KD) in a high AIM2-expressing PDO-T had no effect on proliferation (EdU assays) compared to its empty vector (EV) control PDO-T. By contrast, scratch wound healing assays indicate that the migration potential of the AIM2-KD PDO-T was dramatically impaired (as shown by no significant change in wound area) compared to its EV control PDO-T (significant reduction in wound area) over time (Figure 1C and D). Interestingly, the rate of migration was comparable in the presence (+) or absence (-) of AIM2 agonist polydA:dT, suggesting the PDO-Ts may release DNA-activating ligands in a cell autonomous manner. These observations support the notion that AIM2 is required to augment human GC cell migration during tumorigenesis.

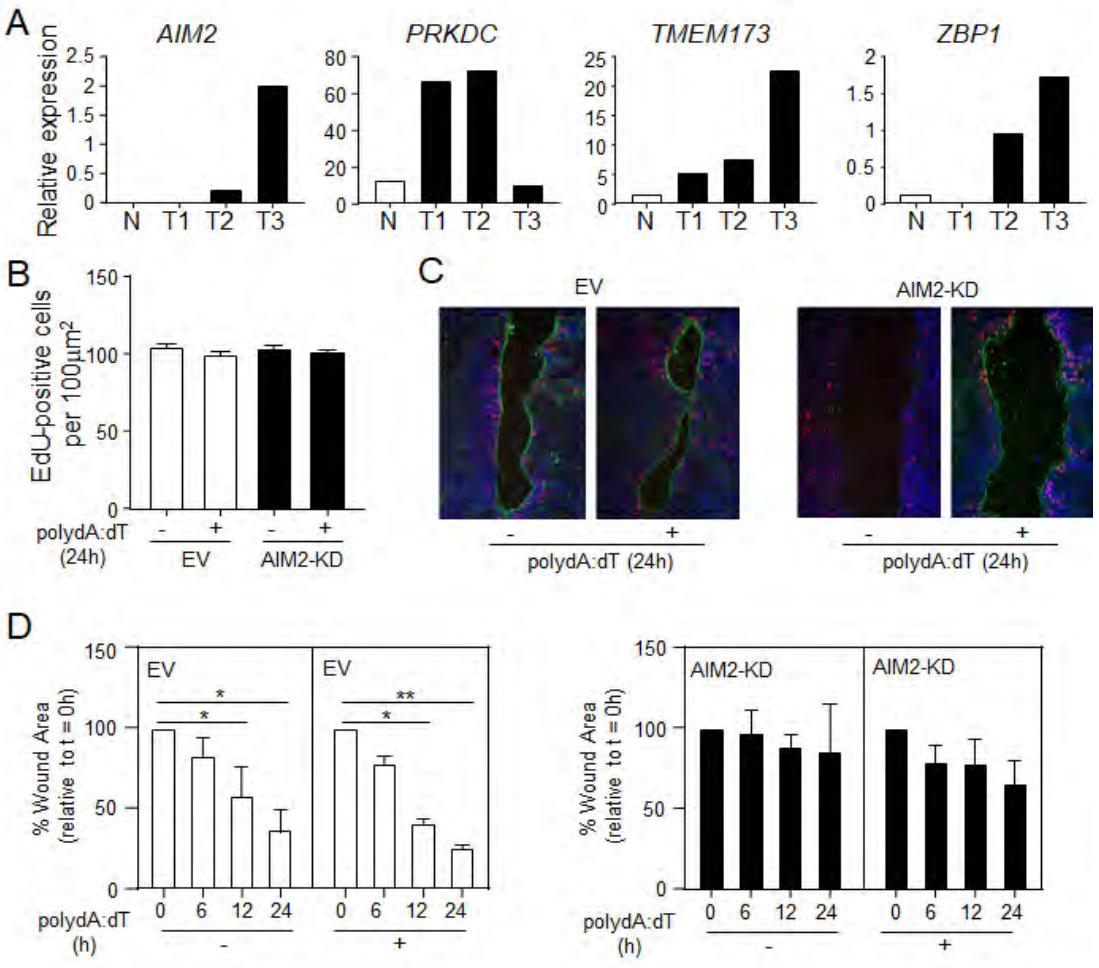

Figure 1. Genetic targeting of AIM2 expression in human gastric cancer patient-derived tumor organoids (PDO-T) impairs cell migration. (A) Gene expression data (RNASeq) of the indicated cytosolic DNA sensors in human GC PDO-Ts from 3 individual patient tumors (T1-T3), along with a control PDO from non-cancerous gastric tissue (N). (B) Proliferation assay (Click-iT EdU) of a PDO-T in which AIM2 was knocked down by CRISPR (AIM2-KD), along with control empty-vector (EV), in the presence or absence of AIM2 agonist poly(dA:dT) over 24 hours (n=3 independent experiments). (C) Representative images of the scratch wound assay on GC PDO-T AIM2-KD and EV epithelial monolayers at 24 hours of culture in the presence or absence of poly(dA:dT). (D) Graphs showing the percentage of wound area (presented as the difference in the percentage of wound area at the indicated hours relative to 0 hour) of the PDO-Ts from panel C. n=3 independent experiments. **P* <0.05, ***P* <0.01; one-way analysis of variance (ANOVA).

In an alternative, yet complementary, approach (see section 5 for rationale), we have also employed our series of human GC cell lines, in which we profiled the same representative DNA sensors for their expression status by qPCR (Figure 2A). Based on our findings for AIM2 in PDO-Ts, we therefore over-expressed AIM2 in the human GC cell line MKN1, and observed that AIM2 over-expression led to a significant increase in the migratory potential of cells independent of the addition of exogenous AIM2 ligand, as determined by transwell migration assays (Figure 2B). This result suggests that AIM2 promotes the migration of human GC cells, which supports our findings in PDO-Ts. Moreover, the protumorigenic role for AIM2 in GC was also demonstrated by the significantly enhanced tumor load in human MKN1 GC cell line xenografts overexpressing AIM2 compared to control (empty vector) MKN1 tumour xenografts (Figure 2C, D).

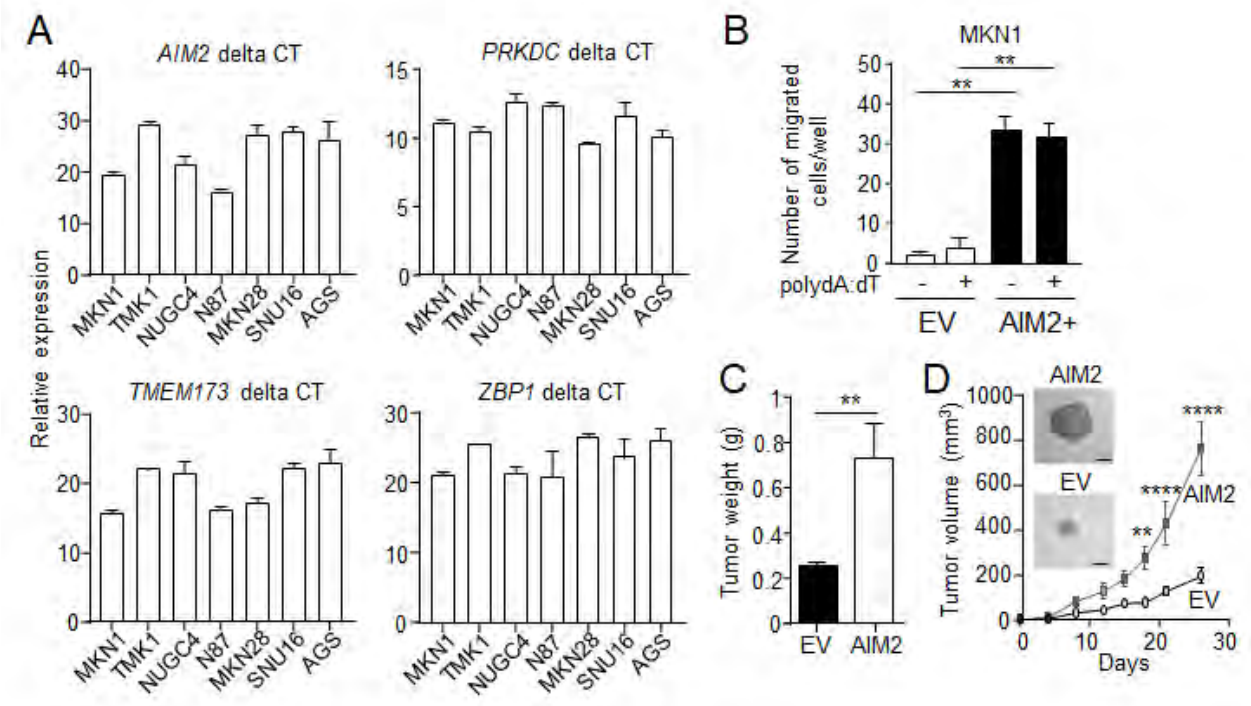

Figure 2. Modulating AIM2 expression augments gastric cancer cell migration. (A) Quantitative real-time (q) PCR expression profiling of the indicated cytosolic DNA sensor genes in human GC cell lines during normal culturing conditions (n = 3 independent passages). Expression data are normalized to the housekeeping gene *18SrRNA* and are presented using the delta Ct

method. (B) Transwell migration assays of mCherry empty vector (EV) and mCherry-tagged AIM2 overexpressing MKN1 cells (AIM2+), in the presence or absence of AIM2 agonist poly(dA:dT) (n=5 independent experiments). ***P* <0.01; one-way analysis of variance (ANOVA). (C, D) Graphs showing (C) tumor weight at day 26 (g), and (D) tumor volume (mm^3) measured every 3-5 days, of EV and AIM2-overexpressing MKN1 xenografts in NOD.Cg-Prkdcscid Il2rgtm1Wjl/SzJ/Arc (NSG) mice (n = 5 mice/group). Also shown in panel (D) are representative images of EV and AIM2-overexpressing xenograft tumors at day 26. Scale bar: 5 mm. ***P* <0.01, *****P* <0.0001; Student's t-test (C) and multiple t-tests (Holm-Sidak method) (D).

Aim 2: despite the initial plan for this work to be undertaken in year 2 (see SOW), we have made substantial progress in this aim already, in particular Major Task 2, Subtasks 1 and 3; this is evidenced by the recent publication of our results and outcomes in the influential journal, *Immunology and Cell Biology* (see "Appendices"). The conclusions from this part of our proposal, as well as a succinct description of the methodology, is also incorporated into this publication.

Specifically, for the AIM2 cytosolic DNA sensor (also guided by our supporting data – Figures 2-4 – in the Project Narrative), we have examined the effect *in vivo* that AIM2 genetic ablation has in our chronic *Helicobacter*-driven gastric pathology mouse model. In *H. felis*-infected *Aim2*$^{-/-}$ mice, histological scoring of mouse stomach sections showed lower levels of inflammatory cell infiltrates compared with infected wild-type (WT) mice (Figure 3A and B). Furthermore, immunohistochemistry revealed a significant decrease in leukocyte/immune cell (CD45+) numbers in *H. felis*-infected *Aim2*$^{-/-}$ stomachs compared with infected WT counterparts (Figure 3C and D). In addition, while *H. felis*-infected WT mice exhibited marked increases in stomach weights and corpus mucosal thickness compared with broth control mice, the stomach weights and corpus mucosal thickness of infected *Aim2*$^{-/-}$ mice were both significantly reduced compared with infected WT mice (Figure 4A-C). Notably, immunohistochemical staining for cellular proliferation with the marker proliferating cell nuclear antigen (PCNA) revealed a significant increase in the numbers of positive cells in both gastric epithelial and immune compartments of *H. felis*-infected WT versus *Aim2*$^{-/-}$ mice (Figure 5A and B). Taken together, these data support a role for AIM2 in driving gastric epithelial and immune cellular proliferation in response to *Helicobacter* infection during the early stages of gastric carcinogenesis.

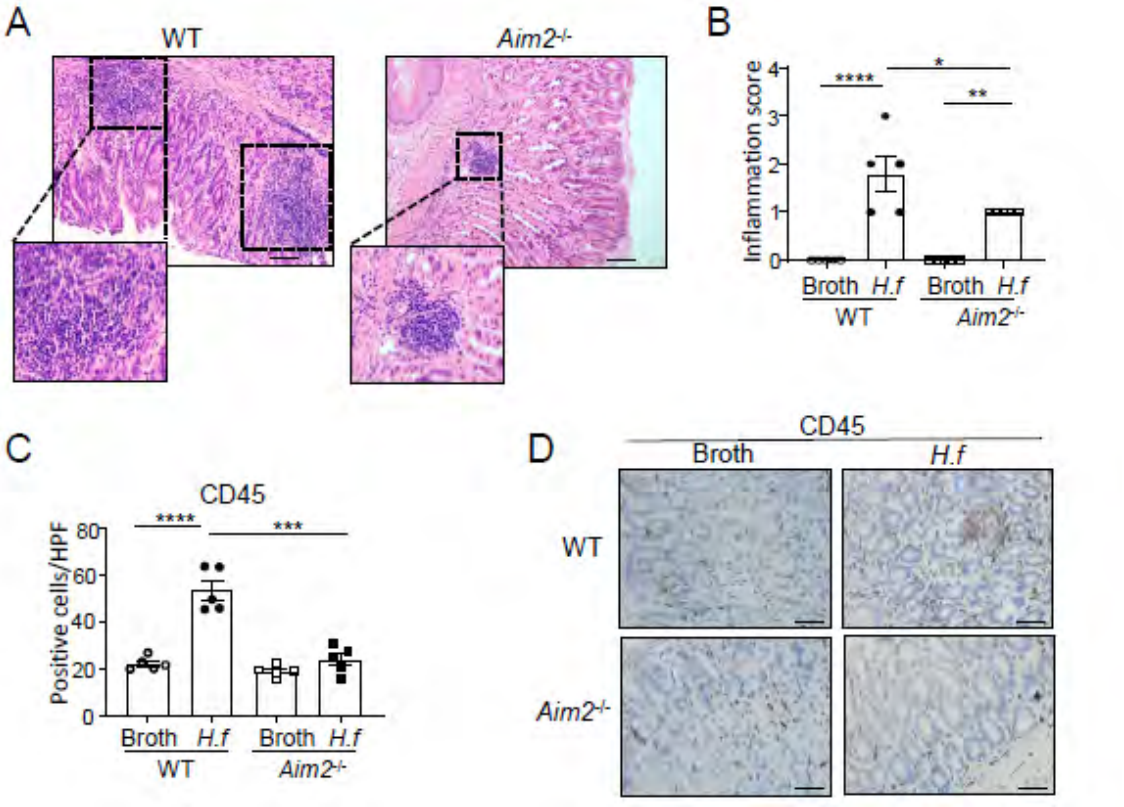

Figure 3: Suppressed inflammation and immune cell infiltrates in stomachs of Aim2-deficient *Helicobacter felis*–infected mice. (A) Representative hematoxylin and eosin–stained *H. felis*-infected WT and *Aim2*$^{-/-}$ mouse stomachs taken at 20x magnification showing immune cell infiltrates. Scale bars = 100 μm. (B) Gastric inflammatory scores (0–3; none, mild, moderate, severe) of WT and *Aim2*$^{-/-}$ mice gavaged with *H. felis* or control broth (n = 8/group). **P* < 0.05, ***P* < 0.01, *****P* < 0.0001; one-way ANOVA with multiple comparisons. (C) Quantification of CD45-positive stained cells in WT and *Aim2*$^{-/-}$ *H. felis*- and broth-gavaged mice (n = 8/group). ****P* < 0.001, *****P* < 0.0001; one-way ANOVA with multiple comparisons. (D) Representative images of CD45 immunostaining in mouse gastric tissue cross-sections from WT and *Aim2*$^{-/-}$ *H. felis*- and broth-gavaged mice. Scale bars = 50 μm.

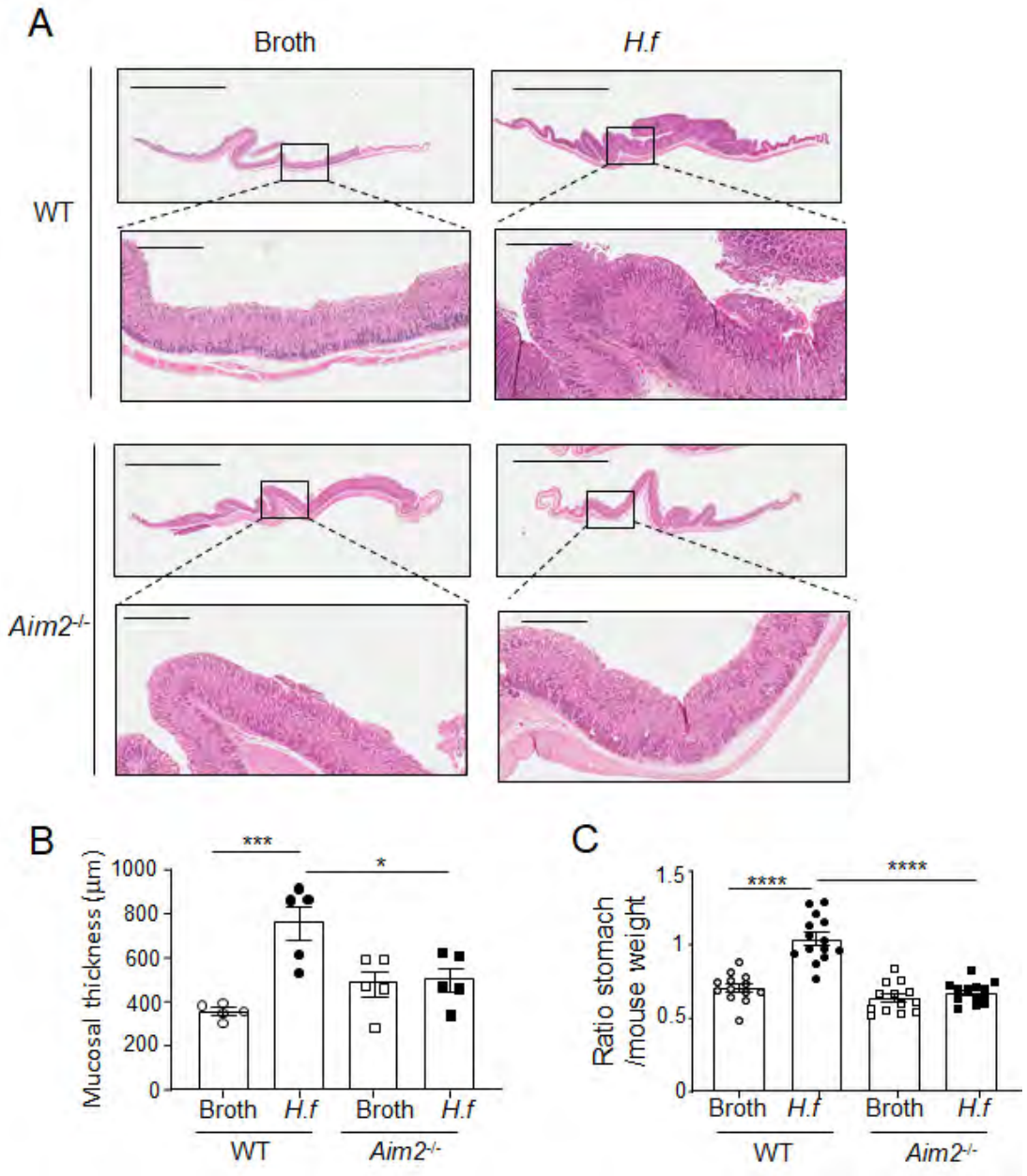

Figure 4. Severity of gastric epithelial hyperplasia is reduced in *Aim2*$^{-/-}$ versus WT *Helicobacter felis*-gavaged mice. (A) Representative images of hematoxylin and eosin–stained WT and *Aim2*$^{-/-}$ mouse gastric tissue cross sections showing mucosal thickness at 4 months post-gavage with *H. felis* or control broth at 0.5x magnification (top panels, scale bars = 5 mm) and 4x magnification (bottom panels, scale bars = 500 μm). (B) Quantification of mucosal thickness of

H. felis and control broth-gavaged WT and *Aim2*$^{-/-}$ mouse gastric corpus (n = 8/group). **P* < 0.05, ****P* < 0.001; one-way ANOVA with multiple comparisons. (C) Ratio of stomach weight to total mouse weight for *H. felis*- and control broth-gavaged WT and *Aim2*$^{-/-}$ mice (n = 13/group). *****P* < 0.0001; one-way ANOVA with multiple comparisons.

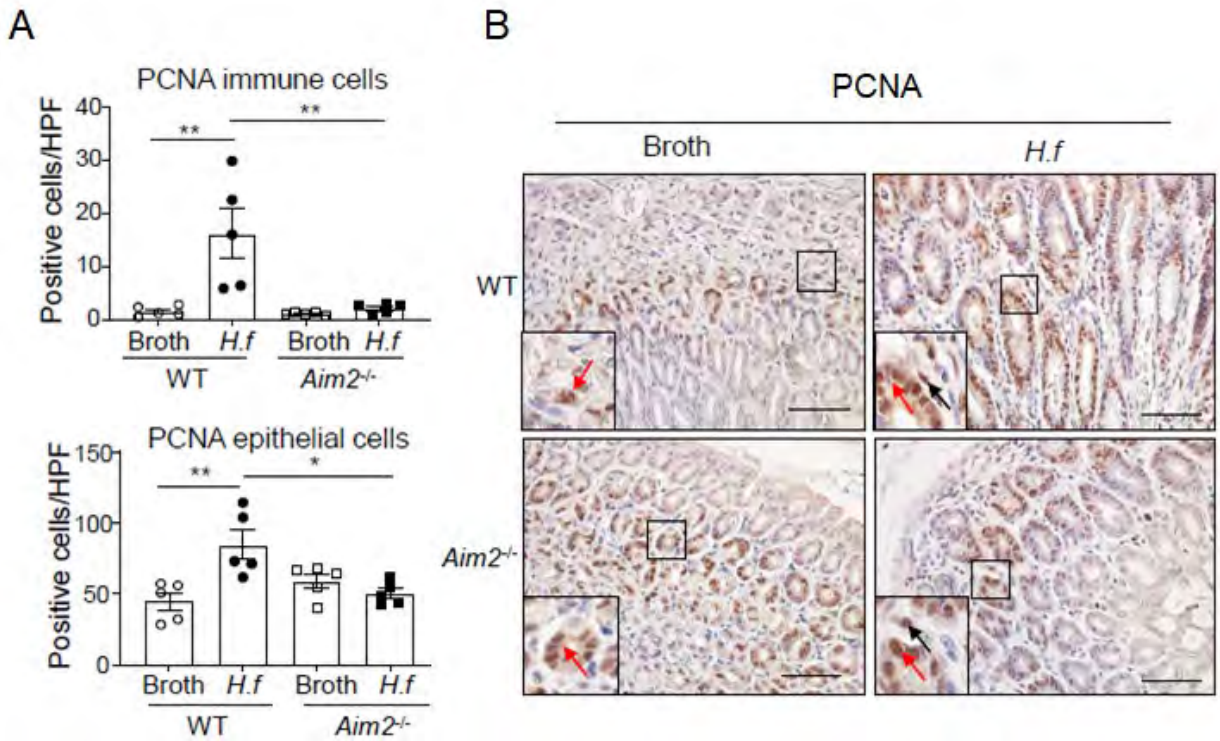

Figure 5. AIM2 promotes proliferation in response to *Helicobacter felis* infection in mouse stomachs (A) Quantification of PCNA immunostained immune cells (top graph) and epithelial cells (bottom graph) in mouse gastric tissue (n = 5/group). **P* < 0.05, ***P* < 0.01; one-way ANOVA with multiple comparisons. (B) Representative images of PCNA immunostaining in mouse gastric tissue. Insets at the bottom left of each image depict magnified areas (open squares) in the main images. Black arrows depict positively stained immune cells, and red arrows depict positively stained epithelial cells, in broth and *H. felis*-gavaged WT and *Aim2*$^{-/-}$ mouse stomach sections. Scale bars = 50 μm. All data were generated using three technical replicates (i.e. triplicates) from a composite of multiple independent experiments.

Opportunities for training and professional development

Dr Ruby Dawson, who was appointed to work on this project as a Post-doctoral Fellow, has participated in several conferences to present talks on our findings thus far. These conference presentations by Dr Dawson are listed below under “Other publications, conference papers, and presentations” in section “6. Products”.

In addition, Dr Dawson has benefited by being invited to join the International Cytokine and Interferon Society (ICIS) as a member of the ICIS Training and Inclusion Committee, as well as being a representative early-career researcher on the ICIS Council (which oversees governance of the ICIS). ICIS is the premier society (1,200 members from over 40 countries) for basic and clinical researchers with an interest in cytokines and interferons, and covers multiple disciplines including cancer, immunology, inflammation and infection. This appointment will provide Dr Dawson with a strong platform to continue her professional development towards an emerging young leader on the world stage.

Dissemination of results to communities of interest

Results from our publication in *Immunology and Cell Biology* were disseminated to lay and research communities via an institutional website, incorporating feeds to social media networks (e.g. Twitter).

Plan to accomplish the goals during the next reporting period

For Aim 1, we will continue to address the current issues regarding the propagation of human gastric organoids (see section 5 below) with a view to performing the planned experiments in Major Task 2/Subtask 2, Major Task 3/Subtasks 1 and 2, and Major Task 4/Subtasks 1-4. As a risk mitigation and alternate approach, in parallel we will continue to also perform the planned experiments in the above-mentioned Major Tasks 2-4 using our panel of human GC cell lines.

For Aim 2, Major Task 2/Subtask 1 upon identifying additional candidate cytosolic DNA sensors we will generate corresponding reporter knockout (KO) mouse strains to assesses their role in promoting *Helicobacter*-driven gastric pathology (as we have successfully done for AIM2).

4. Impact

Development of the principal discipline(s) of the project

During this reporting period, our findings have already had an immediate impact on understanding the importance of cytosolic DNA sensors, in particular AIM2, in the onset of *Helicobacter* infection-driven gastric tumorigenesis. In this respect, the genetic ablation of AIM2 in mice infected with *Helicobacter* suppressed gastric pathology by reducing cellular proliferation and inflammation in the gastric mucosal epithelium. Specifically, AIM2 augmented pathologic proliferative and anti-apoptotic processes in both epithelial and immune cells in the gastric compartment. The disease-promoting role of AIM2 during *Helicobacter* infection was dependent upon its activation via multiprotein 'inflammasome' complexes, thus advancing insights into the dichotomous inflammasome-dependent versus inflammasome-independent activities of AIM2 in pathophysiologic responses. Importantly, evidence for the broad impact of these results and findings on the base of knowledge in the principal disciplinary research fields of cancer, inflammation, gastric disease and innate immunity (incorporating pattern recognition receptors) is evidenced by our recent publication in the broad scope journal *Immunology and Cell Biology* (see "Appendices").

Other disciplines

Uncontrolled activation of AIM2-containing inflammasome complexes is implicated in the development of many infectious (bacterial, viral) and sterile inflammatory diseases, the latter including psoriasis, atherosclerosis and colitis. Furthermore, it is emerging that other cytosolic DNA sensors which act independently of inflammasome complexes, such as STING and cGAS, contribute to the pathogenesis of autoimmune diseases (e.g. rheumatoid arthritis, systemic lupus erythematosus). Collectively, our current findings in this reporting period therefore have potential to impact on research disciplines related to chronic inflammatory conditions and infectious diseases affecting multiple organs.

Technology transfer

Nothing to Report

Society beyond science and technology

Nothing to Report

5. Changes/Problems

Changes in approach and reasons for change

Nothing to Report

Actual or anticipated problems or delays and actions or plans to resolve them

Aim 1 of our research proposal involved the use of human GC patient-derived organoids (PDOs). Despite our initial success (see Figure 1) in propagating (culturing) and experimenting on these organoids – revealing that AIM2 promoted GC cell migration – subsequent attempts to culture PDOs either from fresh or cryopreserved gastric biopsies have been unsuccessful. Around this time, we started to use new batches of several components of the complex media for organoids, and suspect that this may be the reason the organoids have been problematic to grow. We are currently troubleshooting different combinations of reagents for the growth media to try and resolve this issue.

As stated in the Project Narrative, if unforeseen challenges were to arise in generating sufficient PDOs for our study, then an alternative would be to use our series of well-defined human GC cell lines that we have published previously. The use of cell lines can be advantageous because PDOs are not as amenable to high-throughput experimental settings as human GC cell lines due to growth rate variability and higher-level technical requirements. Indeed, our data in Figure 2 (see above) validates this approach since we were able to demonstrate that the genetic modulation of AIM2 expression in the human GC cell line influenced GC cell migration, which supported our findings in a GC PDO (Figure 1). Therefore, we will continue to perform the planned experiments in Aim 1, Major Tasks 2-4 using human GC cell lines in parallel with our ongoing attempts to continue this work also in PDOs.

Changes that had a significant impact on expenditures

Nothing to Report

Significant changes in use or care of human subjects, vertebrate animals, biohazards, and/or select agents

Nothing to Report

Significant changes in use or care of human subjects

Nothing to Report

Significant changes in use or care of vertebrate animals

Nothing to Report

Significant changes in use of biohazards and/or select agents

Nothing to Report

6. Products

Publications, conference papers, and presentations

- Journal publications
  - Dawson RE, Deswaerte V, West AC, Sun E, Wray-McCann G, Livis T, Kumar B, Rodriguez E, Gabay C, Ferrero RL, Jenkins BJ. The cytosolic DNA sensor AIM2 promotes Helicobacter-induced gastric pathology via the inflammasome. *Immunol Cell Biol*. 2023 May;101(5):444-457.
- Books or other non-periodical, one-time publications - Nothing to report
- Other publications, conference papers, and presentations
  - June 2023, Kanazawa University Cancer Research Institute, Kanazawa, Japan. Talk title: Updated perspective on the role of innate immune regulators in upper GI and lung cancers. Presenting author: Brendan Jenkins.

- May 2023, City of Hope, Beckman Research Institute, Duarte, California, USA. Talk title: Updated perspective on the role of innate immune regulators in upper GI and lung cancers. Presenting author: Brendan Jenkins.
- November 2022, Australian Inflammation Centres Symposium, Walter and Elisa Hall Institute, Melbourne, Victoria, Australia. Talk title: The divergent roles of DNA sensor AIM2 in promoting gastric inflammation and tumorigenesis. Presenting author: Ruby Dawson.
- November 2022, Victorian Infection and Immunity Network Young Investigator Symposium, Monash Institute of Pharmaceutical Sciences, Melbourne, Victoria, Australia. Talk title: The divergent roles of DNA sensor AIM2 in promoting gastric inflammation and tumorigenesis. Presenting author: Ruby Dawson.

Website(s) or other Internet site(s)

https://www.hudson.org.au/news/us-defense-dept-backs-aussie-upper-gastrointestinal-cancer-research/

This is an institutional website that disseminates the results of the research activities of PI Brendan Jenkins.

Technologies or techniques

Nothing to report

Inventions, patent applications, and/or licenses

Nothing to report

Other Products

Research material - using CRISPR/Cas9 gene editing, we have knocked down expression of genes encoding cytosolic DNA sensors to evaluate the cellular effects their genetic targeting would have on human GC cell lines and organoids. Therefore, this research tool makes a meaningful contribution toward the understanding of how cytosolic DNA sensors can promote oncogenic cellular processes in human GC cells.

7. Participants and other Collaborating Organizations

Individuals that have worked on the project

Name: Prof Brendan Jenkins
Project Role: Chief Investigator
Researcher Identifier: orcid.org/0000-0002-7552-4656
Nearest person month worked: 3
Contribution to the project: Supervisor of work
Funding Support: Australian National Health and Medical Research Fellowship APP1154279

Name: Dr Ruby Dawson
Project Role: Post-doctoral Fellow
Researcher Identifier: https://orcid.org/0000-0001-9797-7800
Nearest person month worked: 10
Contribution to the project: Performed experiments and analyses
Funding Support: Not applicable

Changes in the active other support of the PD/PI(s) or senior/key personnel since the last reporting period

Nothing to report

Other organizations involved as partners

Monash Health, Melbourne, Victoria, Australia: provides histopathological expertise.

University of Arizona Cancer Center, Tucson, Arizona, USA: provides expertise on human gastric organoids.

8. Special Reporting Requirements

Nothing to report

9. Appendices

See next page onwards for our manuscript recently published in *Immunology and Cell Biology*.

Immunology & Cell Biology 2023; **101**: 444–457
www.wileyonlinelibrary.com/journal/icb

ORIGINAL ARTICLE

OPEN

The cytosolic DNA sensor AIM2 promotes *Helicobacter*-induced gastric pathology *via* the inflammasome

Ruby E Dawson[1,2], Virginie Deswaerte[1,2], Alison C West[1,2], Ekimei Sun[1,2], Georgie Wray-McCann[1,2], Thaleia Livis[1,2], Beena Kumar[3], Emiliana Rodriguez[4], Cem Gabay[4], Richard L Ferrero[1,2,5] & Brendan J Jenkins[1,2]

1 Centre for Innate Immunity and Infectious Diseases, Hudson Institute of Medical Research, Clayton, VIC, Australia
2 Department of Molecular and Translational Science, Faculty of Medicine, Nursing and Health Sciences, Monash University, Clayton, VIC, Australia
3 Department of Anatomical Pathology, Monash Health, Clayton, VIC, Australia
4 Pathology and Immunology Department, CMU/University of Geneva, Geneva, Switzerland
5 Department of Microbiology, Biomedicine Discovery Institute, Monash University, Clayton, VIC, Australia

Keywords
Absent in melanoma 2 (AIM2), gastritis, *Helicobacter*, inflammasome

Correspondence
Brendan J Jenkins, Centre for Innate Immunity and Infectious Diseases, Hudson Institute of Medical Research, Clayton, VIC, Australia.
E-mail: brendan.jenkins@hudson.org.au

Received 11 October 2022;
Revised 14 February and 15 March 2023;
Accepted 24 March 2023

doi: 10.1111/imcb.12641

Immunology & Cell Biology 2023; **101**: 444–457

Abstract

Helicobacter pylori (*H. pylori*) infection can trigger chronic gastric inflammation perpetuated by overactivation of the innate immune system, leading to a cascade of precancerous lesions culminating in gastric cancer. However, key regulators of innate immunity that promote *H. pylori*–induced gastric pathology remain ill-defined. The innate immune cytosolic DNA sensor absent in melanoma 2 (AIM2) contributes to the pathogenesis of numerous autoimmune and chronic inflammatory diseases, as well as cancers including gastric cancer. We therefore investigated whether AIM2 contributed to the pathogenesis of *Helicobacter*-induced gastric disease. Here, we reveal that AIM2 messenger RNA and protein expression levels are elevated in *H. pylori*–positive *versus H. pylori*–negative human gastric biopsies. Similarly, chronic *Helicobacter felis* infection in wild-type mice augmented *Aim2* gene expression levels compared with uninfected controls. Notably, gastric inflammation and hyperplasia were less severe in *H. felis*–infected *Aim2*$^{-/-}$ *versus* wild-type mice, evidenced by reductions in gastric immune cell infiltrates, mucosal thickness and proinflammatory cytokine and chemokine release. In addition, *H. felis*–driven proliferation and apoptosis in both gastric epithelial and immune cells were largely attenuated in *Aim2*$^{-/-}$ stomachs. These observations in *Aim2*$^{-/-}$ mouse stomachs correlated with decreased levels of inflammasome activity (caspase-1 cleavage) and the mature inflammasome effector cytokine, interleukin-1β. Taken together, this work uncovers a pathogenic role for the AIM2 inflammasome in *Helicobacter*-induced gastric disease, and furthers our understanding of the host immune response to a common pathogen and the complex and varying roles of AIM2 at different stages of cancerous and precancerous gastric disease.

INTRODUCTION

Helicobacter pylori (*H. pylori*) is a Gram-negative bacterium which colonizes the stomach and is present in about 50% of the human population. *Helicobacter* infection in the gastric mucosa causes inflammation which, if dysregulated, can lead to the progression of atrophy, metaplasia, dysplasia and eventually intestinal-type gastric adenocarcinoma, the major histopathological type of gastric cancer (GC), or mucosa-associated lymphoid tissue lymphoma.[1–3] Indeed, 1–3% of *H. pylori*–positive patients develop intestinal-type GC,

with about 10% of infected individuals suffering from other clinical complications including peptic ulcers.[4,5] The pathogen–host interaction of *Helicobacter* with the gastric mucosal immune system induces proinflammatory cytokine and reactive oxygen species release, resulting in pathogenic changes to cellular proliferation and homeostasis of the gastric epithelium, and recruitment and migration of immune cells within the stromal compartment.[6–12] However, the molecular basis by which the innate immune system recognizes *Helicobacter* to drive these pathogenic processes is complex and not well understood.

Pattern recognition receptors (PRRs) are a superfamily of regulatory innate immune receptors which can have pro- and anti-inflammatory functions.[13] Among PRRs, the subfamily of Toll-like receptors is the most widely investigated with regard to *Helicobacter* infection.[14–18] Recently, we reported that the endosomal DNA sensor Toll-like receptor 9 is upregulated in both patients with gastritis and GC, and promotes inflammation and proliferation of the gastric mucosal epithelium in a *Helicobacter* infection mouse model.[18] Toll-like receptor 2 has also been shown to recognize *Helicobacter* to activate several signaling pathways and interestingly, was implicated in promoting GC in an inflammation-independent manner.[17,19] Nod-like receptors (NLRs), in particular nucleotide-binding oligomerization domain-containing protein 1 (NOD1), nucleotide-binding oligomerization domain-containing protein 2 (NOD2) and NLR family pyrin domain containing 3 (NLRP3), the latter *via* inflammasome complexes and the interleukin (IL)-1β effector cytokine, have also been reported to contribute to the *Helicobacter*-induced pathogenic inflammatory response involving interferon-gamma production.[10,20] A role for inflammasome-associated inflammation in response to *Helicobacter* was supported through genetic ablation of the inflammasome adaptor, apoptosis-associated speck-like protein containing a CARD (ASC), which reduced inflammation and cytokine release in infected mice.[21] In addition, genetic modulation of IL-1β expression in knockout and transgenic mice has marked effects on *Helicobacter*-induced apoptosis and immune cell infiltration in the gastric mucosal epithelium of mice, suggesting a major role for this inflammasome-associated effector cytokine in *Helicobacter*-induced gastric disease pathogenesis.[22,23] We also note that another inflammasome effector cytokine, IL-18, was found to underpin inflammasome-driven gastric tumorigenesis *via* suppression of apoptosis, independent of inflammation, and may also contribute to early gastric disease pathogenesis.[24] Despite these observations, the full spectrum of PRRs that drive *Helicobacter* pathology remains elusive.

Absent in melanoma 2 (AIM2) is an innate immune cytosolic DNA sensor best known as an inflammasome-associated PRR, and has been implicated in numerous inflammatory diseases and cancers.[13,25] Notably, AIM2 exhibits diverse cellular activities which invariably align with its context-dependent cell and tissue expression, as well as its dual capacity to function both dependent and independent of the inflammasome.[13,25–27] Importantly, a recent study showed that transcriptional upregulation of *Aim2* by the signal transducer and activator of transcription 3 (STAT3) latent oncogenic transcription factor promoted GC *via* a direct, inflammasome-independent role on epithelial cell migration.[28] Conversely, AIM2 was recently implicated in downregulating T-cell–mediated gastritis following *Helicobacter* infection, with the authors suggesting that this was independent of inflammasomes, despite classical read-outs for inflammasome activation (e.g. caspase-1 cleavage) not being assessed.[29] Therefore, whether AIM2 exhibits a potential inflammasome-dependent role in gastric disease pathogenesis remains unclear.

Here, by coupling *bona fide Aim2* knockout mice with a chronic *Helicobacter* infection model, together with clinical biopsies from infected patients, we reveal a driving role for AIM2 in *Helicobacter*-induced gastric pathology. Specifically, AIM2 contributed to augmented proliferation and apoptosis of both gastric epithelial and immune cells upon *Helicobacter* infection. In addition, we show that, mechanistically, AIM2 functions *via* the inflammasome to release the IL-1β effector cytokine. These findings help to unravel the disease-stage dependent and complex roles of AIM2 in gastric disease.

RESULTS

Helicobacter infection upregulates AIM2 expression in human and mouse gastric tissue

To investigate a potential role for AIM2 in the initiating *H. pylori*–driven gastric inflammation stage of gastric carcinogenesis, we first measured *AIM2* gene expression levels by quantitative real-time PCR (qPCR) in patients with gastritis with and without *Helicobacter* infection. Among a range of inflammasome-associated PRRs and the inflammasome adaptor ASCs (encoded by *PYCARD*), only *AIM2* messenger RNA levels were significantly increased (~6-fold) in *H. pylori*–positive *versus H. pylori*–negative gastritis patient biopsies, with *AIM2* also displaying the highest relative expression (Figure 1a). Consistently, immunohistochemical staining for AIM2 revealed more widespread and intense AIM2 positivity in gastric epithelial glandular tissue and immune cells within the lamina propria of *H. pylori*–positive samples than

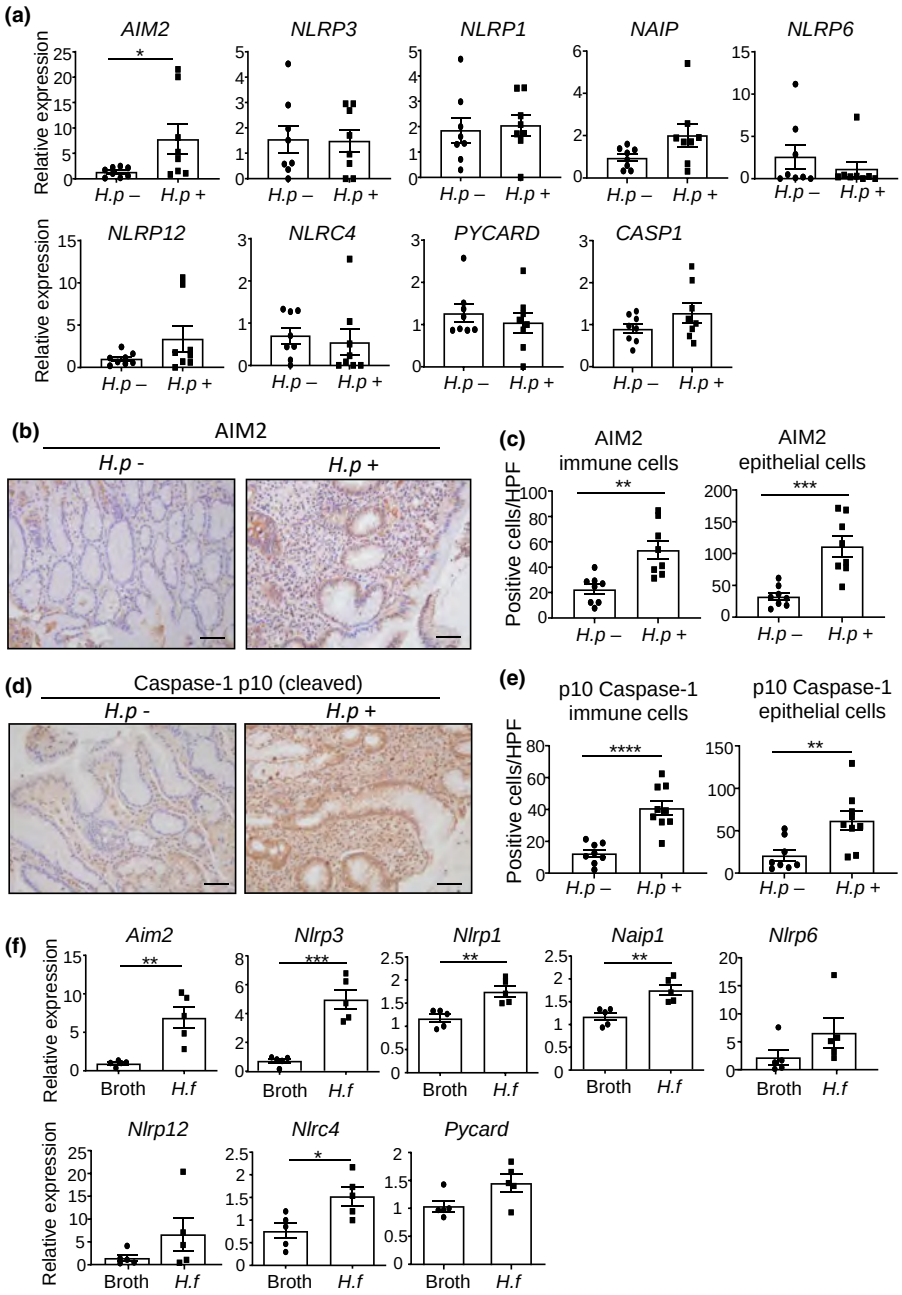

Figure 1. AIM2 expression is increased in gastric biopsies from individuals with *Helicobacter pylori* infection and stomachs of *Helicobacter felis*–infected mice. **(a)** Quantitative real-time PCR expression analysis of PRRs and inflammasome components from *H. pylori*–positive and *H. pylori*–negative patients (n = 8/group). *P < 0.05; Mann–Whitney U-test. Expression data are normalized to the human 18S ribosomal RNA housekeeping gene *RNA18S1*. **(b)** Representative images (40× magnification) of AIM2 immunohistochemistry of the indicated patient gastric biopsies. Scale bars = 50 μm. **(c)** Quantification of AIM2-positive immunostained immune and epithelial cells in patient biopsies (n = 8/group). **P < 0.01, ***P < 0.001; Mann–Whitney U-test. **(d)** Representative images (40× magnification) of cleaved caspase-1 immunohistochemistry of patient gastric biopsies. Scale bars = 50 μm. **(e)** Quantification of cleaved (p10) caspase-1-positive immunostained immune and epithelial cells in patient biopsies (n = 8/group). **P < 0.01, ****P < 0.0001; Mann–Whitney U-test. (**f**) Quantitative real-time PCR expression analysis for PRRs and inflammasome components in gastric tissue of mice gavaged with *H. felis* or control broth (n = 5/group). *P < 0.05, **P < 0.01, ***P < 0.001; Student's t-test. Expression data are normalized to the mouse 18S rRNA housekeeping gene *Rn18s*. All data were generated using three technical replicates (i.e. triplicates) from a composite of multiple independent experiments. AIM2, absent in melanoma 2; CASP1, caspase 1; *H.f*, *H. felis*; *H.p*, *H. pylori*; HPF, high-power field; NAIP, NLR family apoptosis inhibitory protein; NLRC4, NLR family CARD domain containing 4; NLRP1, NLR family pyrin domain containing 1; NLRP3, NLR family pyrin domain containing 3; PRR, pattern recognition receptor; PYCARD, PYD and CARD domain containing.

H. pylori–negative samples (Figure 1b, c). Considering the documented function of AIM2 in inflammasome complexes, we determined whether levels of caspase-1 cleavage, a key indicator of inflammasome activity, was consistent with *Helicobacter* infection status in human gastric biopsies. Indeed, a significant increase in cleaved caspase-1 immunostaining in epithelial and immune cells of *H. pylori*–positive samples was observed, indicating a higher level of inflammasome activity (Figure 1d, e).

To further investigate the effect of *Helicobacter* infection on PRR gene expression, we used a well-established *Helicobacter felis* infection mouse model that reproducibly mimics chronic gastritis and gastric epithelial hyperplasia of *H. pylori* infection in human stomachs.[30] At 4 months following oral gavage with *H. felis*, messenger RNA levels of *Aim2*, along with several other PRRs (*Nlrp3*, *Nlrp1*, *Naip1* and *Nlrc4*), were also elevated in stomachs of *H. felis*–infected mice compared with broth-gavaged control mice, with relative *Aim2* expression the highest (Figure 1f). Taken together, these data suggest that AIM2 is highly upregulated in the stomach among inflammasome-associated PRRs during *Helicobacter* infection.

AIM2 promotes gastric inflammation and immune cell infiltrates in response to *Helicobacter* infection

To determine a functional role for AIM2 in *Helicobacter*-induced gastric pathology, we coupled *Aim2*-deficient mice with the chronic *H. felis* infection model. In *H. felis*–infected $Aim2^{-/-}$ mice, histological scoring of hematoxylin and eosin–stained mouse stomach sections showed lower levels of inflammatory cell infiltrates compared with infected wild-type (WT) mice, with the gastric inflammation score similarly reduced in both male and female *H. felis*–infected $Aim2^{-/-}$ mice (Figure 2a, b, Supplementary figure 1a). Furthermore, immunohisto chemistry revealed a significant decrease (55.67%) in leuko cyte/immune cell ($CD45^{+}$) numbers in *H. felis*–infected $Aim2^{-/-}$ stomachs compared with infected WT co unterparts (Figure 2c, d). Additionally, the increased numbers of T-cell ($CD3^{+}$) and B-cell ($B220^{+}$) infiltrates seen in *H. felis*–infected WT mouse stomachs were markedly reduced in the infected stomachs of $Aim2^{-/-}$ mice for T cells (by 63.34%) and B cells (by 56.72%; Figure 2e, f, Supplementary figure 1b–e). These observatio ns were also supported at the molecular level, whereby qPCR indicated that the increased gastric gene expression levels of a range of proinflammatory cytokines and chemo kines in *H. felis*–infected WT mice (compared with uninfected broth-gavaged WT controls) were significantly reduced in *H. felis*–infected $Aim2^{-/-}$ mice to levels seen in uninfected WT mice (Figure 2g). These data therefore stro ngly suggest that AIM2 deficiency protects mice against *Helicobacter*-induced pathologic inflammatory responses in the stomach.

AIM2 promotes *Helicobacter*-driven gastric epithelial and immune cell proliferation and apoptosis

We next evaluated whether AIM2 also contributed to gastric epithelial hyperplasia, evidenced by augmented mucosal thickness of the gastric corpus, that is a feature of chronic *Helicobacter* infection.[31] Notably, while *H. felis*–infected WT mice exhibited marked increases in stomach weights (56.75%) and corpus mucosal thickness (96.97%) compared with broth control mice, the stomach weights and corpus mucosal thickness of infected $Aim2^{-/-}$ mice were significantly reduced by 35.90% and 31.07%, respectively, compared with infected WT mice (Figure 3a–c). These observed reductions in stomach weights and corpus mucosal thickness of infected $Aim2^{-/-}$ *versus* WT mice were similar among both males and females, suggesting that AIM2 promotes gastric hyperplasia irrespective of gender (Supplementary figure 2a, b). The suppressed *H. felis*–driven gastric pathology in $Aim2^{-/-}$ mice was not because of the inability of *H. felis* to colonize mouse stomachs, as qPCR expression analysis of the *H. felis*–specific *flaB* gene showed that the gastric corpus bacterial loads of *H. felis* were similarly increased in both WT and $Aim2^{-/-}$ infected mice compared with their uninfected counterparts (Figure 3d).

In addition, immunohistochemical staining for markers of cellular proliferation, proliferating cell nuclear antigen (PCNA) and Ki67, revealed a significant increase in the numbers of positive cells in both gastric epithelial and immune compartments of *H. felis*–infected WT *versus* $Aim2^{-/-}$ mice (Figure 4a–d). Importantly, immunofluorescence costaining of PCNA with the epithelial marker, E-cadherin, and the pan-immune cell marker, CD45, confirmed pronounced colocalization of PCNA positivity in both epithelial and immune cells of *H. felis*–infected WT mice compared with $Aim2^{-/-}$ mice (Supplementary figure 3a, b). These data therefore support a role for AIM2 in driving gastric epithelial and immune cellular proliferation in response to *Helicobacter* infection.

We next evaluated the effect of *Helicobacter* infection on gastric cellular apoptosis by performing immunohistochemistry and immunofluorescence analyses for markers of apoptosis, TUNEL (terminal deoxynucleotidyl transferase dUTP nick end labeling) and cleaved caspase-3, respectively. Indeed, the increased numbers of TUNEL-positive apoptotic cells observed in *H. felis*–infected WT mouse stomachs (compared with broth WT controls) were significantly reduced in *H. felis*–

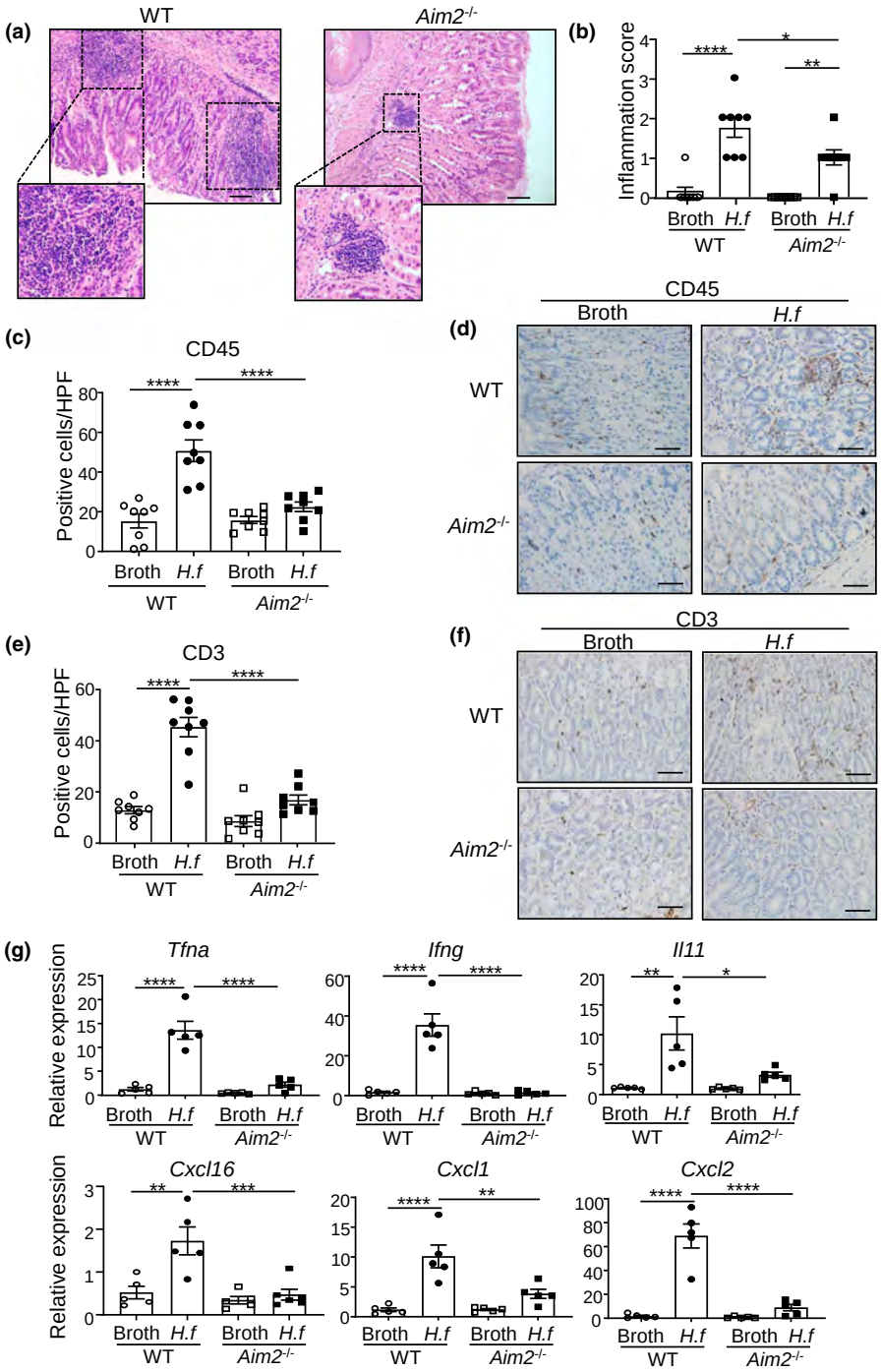

Figure 2. Suppressed inflammation and immune cell infiltrates in stomachs of *Aim2*-deficient *Helicobacter felis*–infected mice. **(a)** Representative hematoxylin and eosin–stained *H. felis*–infected WT and *Aim2*$^{-/-}$ mouse stomachs taken at 20× magnification showing immune cell infiltrates. Scale bars = 100 μm. **(b)** Gastric inflammatory scores (0–3; none, mild, moderate, severe) of WT and *Aim2*$^{-/-}$ mice gavaged with *H. felis* or control broth (n = 8/group). *P < 0.05, **P < 0.01, ****P < 0.0001; one-way ANOVA with multiple comparisons. **(c, e)** Quantification of CD45-positive (**c**) and CD3-positive (**e**) stained cells in WT and *Aim2*$^{-/-}$ *H. felis*– and broth-gavaged mice (n = 8/group). ****P < 0.0001; one-way ANOVA with multiple comparisons. **(d, f)** Representative images of CD45 **(d)** and CD3 **(f)** immunostaining in mouse gastric tissue cross-sections from WT and *Aim2*$^{-/-}$ *H. felis*– and broth-gavaged mice. Scale bars = 50 μm. **(g)** Quantitative real-time PCR expression analysis of proinflammatory cytokines in *H. felis*– or broth-gavaged WT and *Aim2*$^{-/-}$ mouse gastric tissues (n = 5/group). *P < 0.05, **P < 0.01, ***P < 0.0001, ****P < 0.0001; one-way ANOVA with multiple comparisons. All data were generated using three technical replicates (i.e. triplicates) from a composite of multiple independent experiments. AIM2, absent in melanoma 2; *H.f*, *H. felis*; WT, wild type.

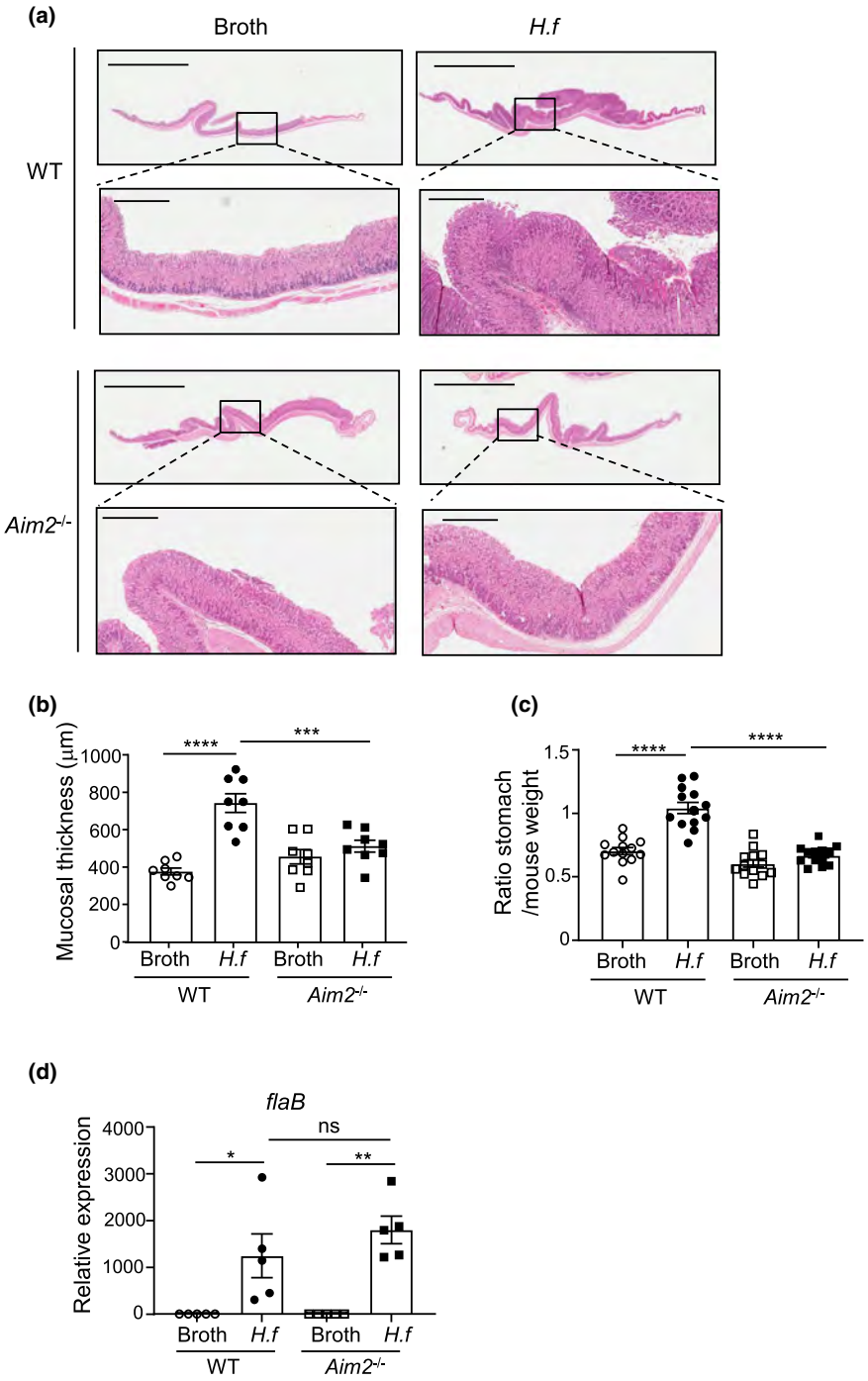

Figure 3. Severity of gastric epithelial hyperplasia is reduced in *Aim2*$^{-/-}$ *versus* WT *Helicobacter felis*–gavaged mice. **(a)** Representative images of hematoxylin and eosin–stained WT and *Aim2*$^{-/-}$ mouse gastric tissue cross sections showing mucosal thickness at 4 months postgavage with *H. felis* or control broth at 0.5× magnification (top panels, scale bars = 5 mm) and 4× magnification (bottom panels, scale bars = 500 μm). **(b)** Quantification of mucosal thickness of *H. felis* and control broth–gavaged WT and *Aim2*$^{-/-}$ mouse gastric corpus (n = 8/group). ***P < 0.001, ****P < 0.0001; one-way ANOVA with multiple comparisons. **(c)** Ratio of stomach weight to total mouse weight for *H. felis*– and control broth–gavaged WT and *Aim2*$^{-/-}$ mice (n = 13/group). ****P < 0.0001; one-way ANOVA with multiple comparisons. **(d)** *H. felis* colonization of corpus tissue determined by quantitative real-time PCR gene expression for *H. felis*–specific *flaB* (relative to mouse *18S*) in genomic DNA of stomachs from the indicated WT and *Aim2*$^{-/-}$ mouse groups (n = 5/group). All data were generated using three technical replicates (i.e. triplicates) from a composite of multiple independent experiments. *P < 0.05; **P < 0.01; one-way ANOVA with multiple comparisons. ns, not significant. AIM2, absent in melanoma 2; *H.f*, *H. felis*; WT, wild type.

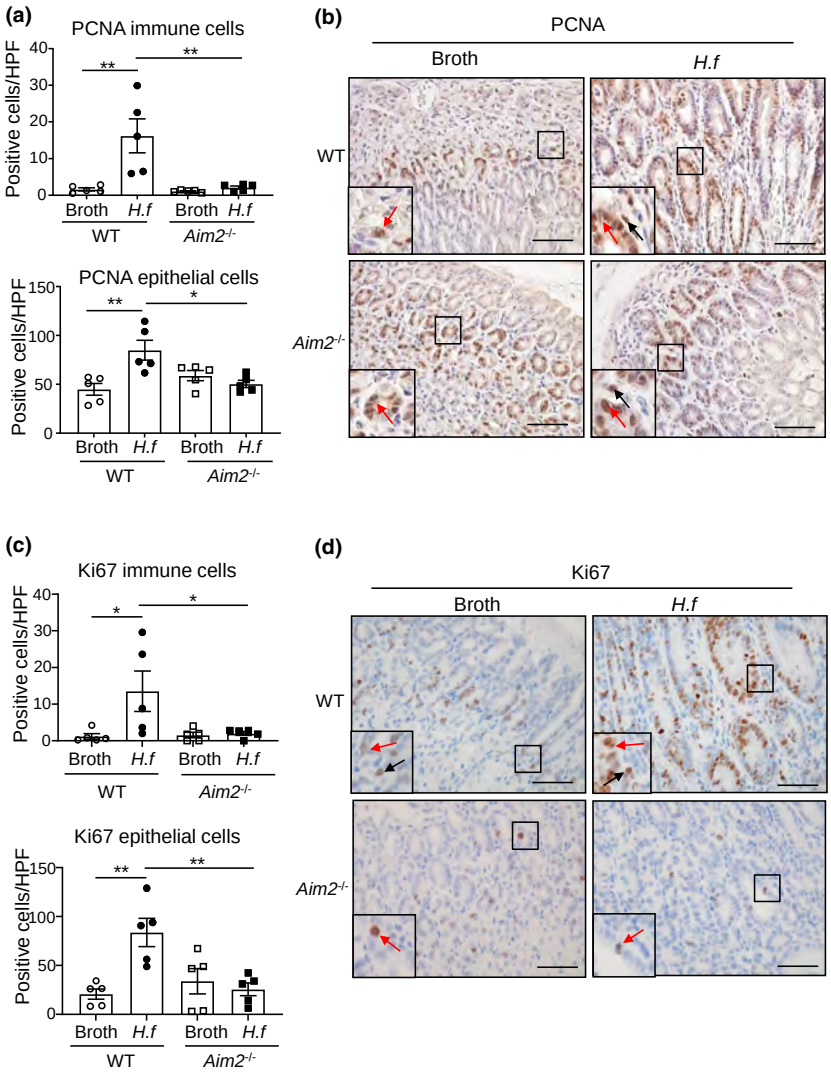

Figure 4. AIM2 promotes proliferation in response to *Helicobacter felis* infection in mouse stomachs **(a, c)**. Quantification of PCNA **(a)** and Ki67 **(c)** immunostained immune cells (top graph) and epithelial cells (bottom graph) in mouse gastric tissue (n = 5/group). *P < 0.05, **P < 0.01; one-way ANOVA with multiple comparisons. **(b, d)** Representative images of **(b)** PCNA and **(d)** Ki67 immunostaining in mouse gastric tissue. Insets at the bottom left of each image depict magnified areas (open squares) in the main images. Black arrows depict positively stained immune cells, and red arrows depict positively stained epithelial cells, in broth and *H. felis*–gavaged WT and *Aim2*$^{-/-}$ mouse stomach sections. Scale bars = 50 μm. All data were generated using three technical replicates (i.e. triplicates) from a composite of multiple independent experiments. AIM2, absent in melanoma 2; *H.f*, *H. felis*; HPF, high-power field; PCNA, proliferating cell nuclear antigen.

infected *Aim2*$^{-/-}$ mice in both gastric epithelial cells (by 48.93%) and immune cell infiltrates (by 61.39%) (Figure 5a, b). Similarly, immunofluorescence indicated a 68.54% and 46.43% reduction in the numbers of cleaved caspase-3 positively stained apoptotic gastric epithelial cells and immune cell infiltrates, respectively, in the stomachs of *H. felis*–infected *Aim2*$^{-/-}$ mice *versus* WT mice (Figure 5c, d). Collectively, the suppressed pathologic proliferative and apoptotic epithelial and immune cellular responses in the gastric compartment of *Helicobacter*-infected *Aim2*$^{-/-}$ mice suggest that AIM2 contributes to gastric pathology *via* modulating these cellular functions throughout the inflamed gastric mucosa.

AIM2 functions *via* the inflammasome to promote gastric pathology during *Helicobacter* infection

Considering AIM2 has a well-known function in the formation of inflammasome complexes, we next assessed whether AIM2 deficiency would impair the activation levels of the key inflammasome effector, caspase-1,

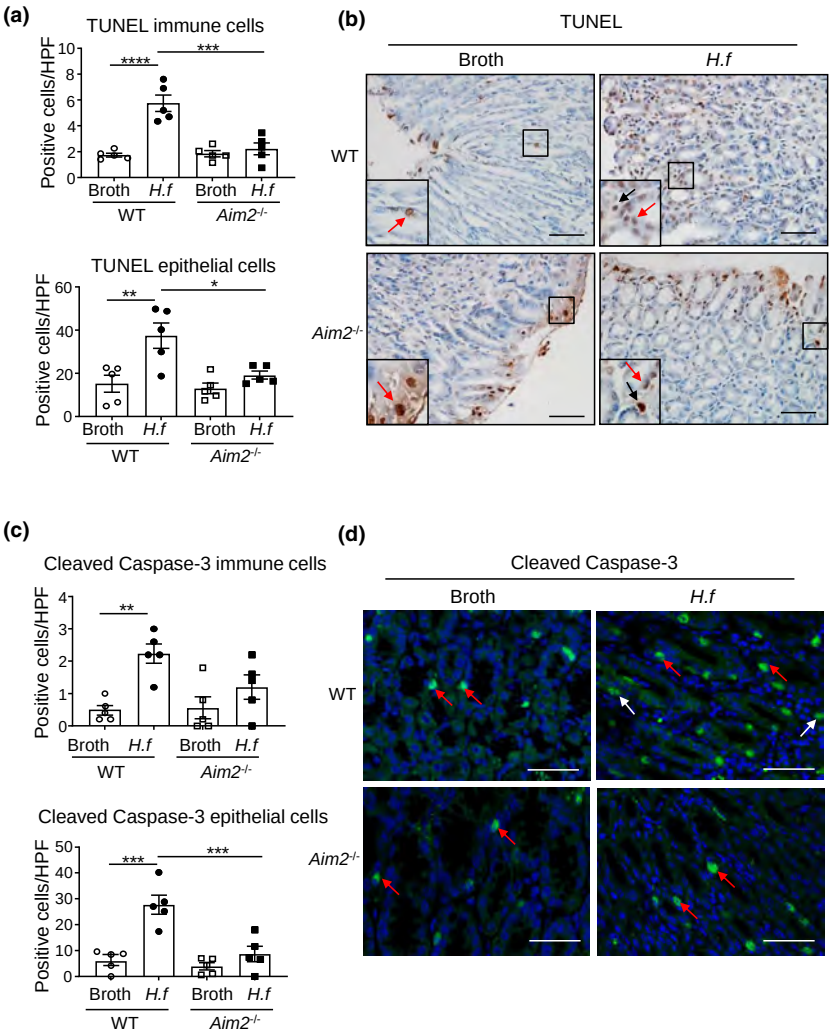

Figure 5. *Aim2* promotes apoptosis in response to *Helicobacter felis* infection in mouse stomachs. **(a)** Quantification of TUNEL-immunostained immune cells (top graph) and epithelial cells (bottom graph) in mouse gastric tissue cross sections (n = 5/group). *P < 0.05, **P < 0.01, ***P < 0.001, ****P < 0.0001; one-way ANOVA with multiple comparisons. **(b)** Representative images of TUNEL immunostaining in mouse gastric tissue cross sections. Insets at the bottom left of each image depict magnified areas (open squares) in the main images. In insets, black arrows depict positively stained immune cells, and red arrows depict positively stained epithelial cells, in broth- and *H. felis*–gavaged WT and *Aim2*$^{-/-}$ mouse stomach sections. Scale bars = 50 μm. **(c)** Quantification of cleaved caspase-3 immunofluorescence-positive immune cells and epithelial cells in mouse gastric tissue cross sections (n = 5/group). **P < 0.01, ***P < 0.001; one-way ANOVA with multiple comparisons. **(d)** Representative images of cleaved caspase-3 immunofluorescence (green) plus DAPI nuclear staining (blue) in mouse gastric tissue cross sections. Red arrows depict positively stained epithelial cells and white arrows depict positively stained immune cells. Scale bars = 50 μm. All data were generated using three technical replicates (i.e. triplicates) from a composite of multiple independent experiments. AIM2, absent in melanoma 2; DAPI, 4′,6-diamidino-2-phenylindole; *H.f*, *H. felis*; HPF, high-power field; TUNEL, terminal deoxynucleotidyl transferase dUTP nick end labeling; WT, wild type.

during chronic *Helicobacter* infection. Indeed, immunohistochemistry revealed there were higher levels of cellular (immune and epithelial) staining for the mature, cleaved (i.e. activated) form of caspase-1 (p10) in gastric tissue cross sections from *H. felis*–infected WT compared with *Aim2*$^{-/-}$ mice, irrespective of gender (Figure 6a, b, Supplementary figure 4a, b). In addition, immunoblotting together with densitometric quantification for caspase-1 protein expression showed increased amounts of the cleavage product (p20), as well as the immature proform (p45), of caspase-1, in gastric tissue lysates of *H. felis*–infected WT mice compared with *H. felis*–infected *Aim2*$^{-/-}$ mice (Figure 6c–e). Interestingly, while basal gastric levels of p20 and p45 caspase-1 forms appeared elevated in broth control *Aim2*$^{-/-}$ compared with WT mice, this did not equate to

an increase in the relative cleavage of the p45 proform to the mature/activated p20 form (based on the p20/p45 ratio; Figure 6c–e). In addition, messenger RNA levels of caspase-1 were diminished in *H. felis*–infected *Aim2*$^{-/-}$ mice compared with *H. felis*–infected WT mice (Figure 6f). These findings suggesting that AIM2 is associated with inflammasome complexes during chronic *Helicobacter* infection were further supported by our observations that secreted circulating protein levels of the bioactive form of the inflammasome effector cytokine, IL-1β, were elevated in serum of *H. felis*–infected WT mice compared with broth controls, while serum IL-1β protein levels were decreased in *H. felis*–infected *Aim2*$^{-/-}$ mice, as measured by ELISA (Figure 6g). By contrast, serum protein levels of the other major inflammasome effector cytokine, IL-18, were undetectable by ELISA (data not shown). Overall, these data support our findings of *Helicobacter*-associated elevated inflammasome activity in human gastric tissue biopsies, and suggest that AIM2 *via* inflammasomes promotes *Helicobacter*-induced gastric disease.

DISCUSSION

The host immune response to *Helicobacter* infection in the stomach is a critical determinant in the extent and severity of gastric inflammation and subsequent risk of GC. While members of the innate immune Toll-like receptor and NLR families have been extensively investigated in the early stages of *Helicobacter* infection and gastric disease, here we focused on the cytosolic DNA sensor, AIM2. Our investigation revealed that AIM2 was critical for promoting *Helicobacter*-induced chronic gastric pathology comprising inflammation and epithelial hyperplasia, *via* altering proliferation and apoptosis of gastric epithelial and immune cells, recruitment of immune cells and production of proinflammatory cytokines and chemokines.

A key finding of our study was that AIM2 messenger RNA and protein levels were upregulated in *H. pylori*–positive human gastric biopsies and gastric tissues from *H. felis*–infected mice, consistent with inflammasome activity. Interestingly, this contrasts recent findings that other DNA sensors, namely, stimulator of interferon genes (STING) and retinoid acid inducible gene I (RIG-I), are downregulated by *Helicobacter* in an 8-week infection mouse model where deletion of *Sting1* or *Rigi* reduced acute immune responses but not chronic gastric inflammation.[32] The expression of both these genes also negatively correlates with GC prognosis in patients.[32–34] This contrasts that of AIM2, whose upregulated expression in patients with GC correlates with impaired survival.[28] Furthermore, in a hyperinflammatory mouse model of spontaneous GC driven by deregulated cytokine signaling *via* the IL-11/STAT3 axis, we recently reported that AIM2 promotes the progression of GC independent of the inflammasome and inflammation, but rather by augmenting intrinsic epithelial cell migration.[28] While this contrasts our current findings that the AIM2 inflammasome promotes *Helicobacter*-driven gastric inflammation, these findings nonetheless suggest a dichotomous role for AIM2 in which it promotes early stage *Helicobacter* infection–driven gastritis in an inflammasome-dependent manner, and late-stage cytokine–driven gastric tumorigenesis independent of inflammasomes. A possible explanation for the divergent functions of AIM2 in gastric disease is the cell-type context of its expression. Indeed, in GC, AIM2 upregulation was tumor intrinsic and restricted to the gastric epithelium, while we demonstrate here that AIM2 is upregulated in both gastric epithelial and immune cells in early stage *Helicobacter*-related gastritis.[28] We also note that an inflammasome-independent role for AIM2 that is intrinsic to the gut epithelium has been demonstrated in colon cancer, whereby AIM2 suppresses intestinal tumorigenesis in Apc$^{Min/+}$ and DSS/AOM mouse models by modulating intestinal epithelial cell apoptosis and proliferation.[25,35] While these observations suggest that inflammasome-independent roles for AIM2 in gastrointestinal pathologies predominantly align with AIM2 expression and function in the epithelium, it is also noteworthy that AIM2 inflammasome activity intrinsic to the gut epithelium has been attributed to the regulation of intestinal homeostasis in mouse models of colitis in both epithelial and macrophages, specifically *via* IL-18 production.[27,36] Therefore, the complex context dependency of AIM2 pathophysiological functions and molecular mechanisms (i.e. inflammasome dependent *versus* independent) in the gastrointestinal tract are likely underpinned by not only its expression in specific cell types (i.e. epithelial *versus* immune), but also tissue types and disease stage, as well as the type (i.e. endogenous *versus* microbial) and subcellular location (i.e. cytosol *versus* nucleus) of activating ligands. Importantly, considering these complexities regarding AIM2 biological functions in gastrointestinal pathologies, future studies are warranted to couple conditional knockout strains of AIM2 with gastrointestinal disease models (including *Helicobacter* infection) to identify specific AIM2-expressing cell types that modulate disease pathogenesis.

We also observed that AIM2 promoted proliferation and apoptosis in both gastric epithelial and immune cells, which suggests that disrupted cellular homeostasis may be a key mechanism underlying *Helicobacter*-related pathology. Dysregulated epithelial cell proliferation is often associated with inflammation throughout the gastrointestinal system

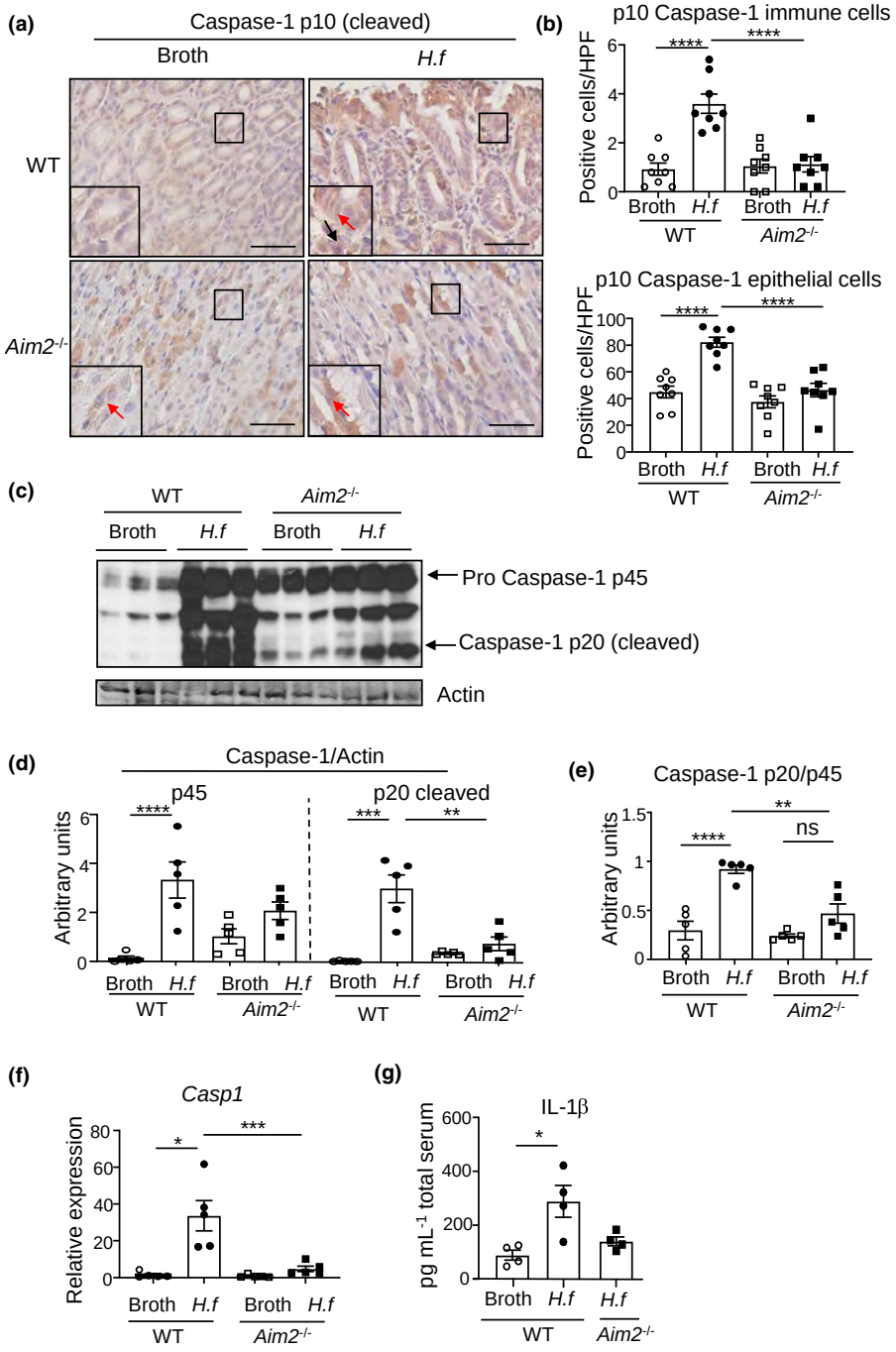

Figure 6. Suppressed inflammation in *Aim2*$^{-/-}$ *Helicobacter felis* mouse stomachs correlates with reduced inflammasome activity. **(a)** Representative images of cleaved caspase-1 immunostaining in gastric tissue sections from broth- and *H. felis*–gavaged WT and *Aim2*$^{-/-}$ mice. Red arrows depict positively stained epithelial cells and black arrows depict positively stained immune cells. Scale bars = 50 μm. **(b)** Quantification of positively immunostained cleaved (p10) caspase-1 immune cells (top graph) and epithelial cells (bottom graph) in the indicated mouse gastric tissue groups (n = 8/group). ****P < 0.0001; one-way ANOVA with multiple comparisons. **(c)** Immunoblot for caspase-1 showing cleaved (p20) and pro (p45) forms of the protein indicated with arrows. Each lane represents an individual mouse sample. Actin is used as a loading control. **(d, e)** Semiquantitative densitometry of the relative expression of cleaved and pro forms of caspase-1 normalized to actin **(d)**, and cleaved caspase-1 normalized to procaspase-1 **(e)** (n = 5/group). **P < 0.01, ***P < 0.001, ****P < 0.0001; one-way ANOVA with multiple comparisons. ns, not significant. **(f)** Quantitative real-time PCR expression analysis for *Casp1* in *H. felis*– or broth-gavaged WT and *Aim2*$^{-/-}$ mouse gastric tissues (n = 5/group). *P < 0.05, ***P < 0.001; one-way ANOVA with multiple comparisons. **(g)** ELISA for IL-1β on *H. felis*– *versus* broth-gavaged WT, and *H. felis*–gavaged *Aim2*$^{-/-}$, mouse serum (n = 4/group). *P < 0.05; Student's t-test. All data were generated using three technical replicates (i.e. triplicates) from a composite of multiple independent experiments. AIM2, absent in melanoma 2; *H.f*, *H. felis*; IL, interleukin; WT, wild type.

and it has been documented that *Helicobacter* alters both proliferation and apoptosis of gastric cells.[37,38] We speculate that dysregulation of epithelial cell homeostasis by upregulation of AIM2 results in loss of barrier integrity which exacerbates the inflammatory response as the underlying tissue is more exposed to *Helicobacter* and other pathogens. The role of AIM2 in barrier function has been reported in the context of *Salmonella* infection in the colon, albeit with its expression having an opposing effect (i.e. promoting barrier integrity).[39] The differences in AIM2 on gastric and intestinal disease further exemplify the diverse roles of AIM2 and suggest that the gastrointestinal tract may be finely tuned to a physiological threshold of AIM2 expression/activation for homeostasis whereby disrupting this balance compromises integrity.

We also refer our current findings to a recent study suggesting that AIM2 independent of inflammasomes has a protective role against *Helicobacter*-induced gastric inflammation and associated spasmolytic peptide-expressing metaplasia. Specifically, using a 6-month *H. felis* infection spasmolytic peptide-expressing metaplasia mouse model, AIM2 was proposed to selectively suppress the recruitment of interferon-gamma–producing gastric $CD8^+$ T cells (along with impaired expression of key T-cell homing receptors; e.g. Selectin L, Sphingosine-1-Phosphate Receptor 1) *via* a B-cell–intrinsic function that blocked production of the T-cell chemoattractant, chemokine (C–X–C motif) ligand 16.[29] These observations contrast our study, where we also did not observe any changes in expression of either interferon-gamma, chemokine (C–X–C motif) ligand 16 or T-cell homing receptors (Supplementary figure 5) in the stomachs of infected $Aim2^{-/-}$ mice. In considering an explanation for the opposing observations of these two studies, it is important to note that El-Zaatari and colleagues employed *Aim2* gene-trap mice, which express residual AIM2, unlike our current study that employed *bona fide* whole-body AIM2-deficient mice.[28,29,40,41] Furthermore, the suggestion that AIM2 acted independent of inflammasomes was limited to assessment of only (unaltered) protein levels of IL-18 and IL-1β secreted from *ex vivo* gastric explants of WT and *Aim2* gene-trap mice, with no *in vivo* assessment of protein levels of mature forms of these inflammasome effector cytokines, nor levels of cleaved (i.e. active) caspase-1, a hallmark of AIM2 inflammasome activity.[29] We also note the possibility that these studies, which employ *H. felis* infections over different periods (i.e. 4 months *versus* 6 months), may further uncover multiple, and potentially contrasting, roles for AIM2 during various stages (e.g. gastritis, metaplasia) of chronic *Helicobacter* infection. In this respect, in addition to AIM2, several other inflammasome-associated components (*via* IL-1β) that have been reported to contribute to gastric inflammation and pathology in *Helicobacter* infection mouse models, namely ASC and NLRP3,[10,21,42] also play contrasting roles within a specific disease setting that are dependent on expression in specific cell types and stages of disease.[43–46]

In summary, our current study suggests that the AIM2 inflammasome is a critical regulator of inflammation in the earlier stages of *Helicobacter*-induced gastritis and associated epithelial hyperplasia. Coupled with the finding that AIM2 can also act independent of inflammasomes to promote later stage gastric adenocarcinoma, these observations expand our current understanding of the complexities of AIM2 function during the cascade of events and immunoregulatory checkpoints that underpin gastric carcinogenesis. Furthermore, these inflammasome-dependent (early stage gastritis) and inflammasome-independent (late stage gastric adenocarcinoma) mechanism(s) of action of AIM2 have potential to guide distinct therapeutic strategies against AIM2 at specific stages of the gastric carcinogenesis cascade.

METHODS

Patient biopsies

Gastric body samples were collected from patients with non-GC undergoing endoscopy at Monash Medical Centre (Melbourne, VIC, Australia; Supplementary table 1). Exclusion criteria included individuals with serious concomitant illness, observable tumors, gastrointestinal bleeding, previous gastric surgeries and prior use of proton pump inhibitors, antibiotics or nonsteroidal anti-inflammatory drugs. Biopsies were either snap-frozen in liquid nitrogen or stored in 10% formalin, the latter for histopathology.[47] The *H. pylori* status was determined by *16S* rRNA qPCR and assessment of Cresyl fast violet–stained tissue sections as described before.[31] We note that the etiology of *H. pylori*–negative gastritis is poorly understood, and likely to involve overgrowth of other pathogenic microbes (e.g. *Streptococcus*).[48,49] Written informed consent was obtained from each patient, and biopsy collections were approved by the Monash Health Human Research Ethics Committee. Patient studies were conducted in accordance with the World Medical Association Declaration of Helsinki statement on the ethical principles for medical research involving human subjects.

Mice

Aim2-knockout ($Aim2^{-/-}$) mice on a mixed C57BL6 × 129Sv background have been previously described,[28,40] and genetically matched WT littermates were used as controls. Where possible, equal numbers of male and female mice were randomly assigned to experimental groups. All animals were housed under specific pathogen-free conditions, and studies were approved by the Monash University Monash Medical Centre "B" Animal Ethics Committee.

In vivo H. felis infection model

Helicobacter felis (strain CST1)[50,51] was cultured and harvested on horse blood agar or brain heart infusion broth. *H. felis* suspensions for mouse inoculations were prepared from bacteria on horse blood agar plates using brain heart infusion broth.[30] Four- to six-week-old WT or *Aim2*$^{-/-}$ mice were administered with either control brain heart infusion broth or approximately 10^7 *H. felis* bacterial suspension by single oral gavage (200 µL) using polyethylene catheters.[31] Mice were culled at 4 months after infection for subsequent analyses. *H. felis* bacterial loads were confirmed using qPCR amplification of the *H. felis flab* gene as previously described.[31]

Gene expression analyses

Equivalent amounts of total RNA were isolated from *Helicobacter*-positive and *Helicobacter*-negative snap-frozen mouse (100 mg) and human (100 mg) stomach tissue biopsies using TRI Reagent Solution (Sigma-Aldrich, St Louis, MO, USA), followed by on-column RNeasy Mini Kit RNA clean-up and DNase treatment (Qiagen, Hilden, Germany). Total RNA was then reverse transcribed (1 µg in 20 µL reaction volume for each RNA sample) with the Transcriptor High Fidelity cDNA Synthesis Kit (Sigma-Aldrich). Each qPCR was performed on 2 µL diluted complementary DNA (diluted 1:10 for mouse, 1:5 for human samples) with SYBR Green chemistry (Life Technologies, Carlsbad, CA, USA) and a final primer concentration of 2 µM using the QuantStudio 6 Flex Real-Time PCR System (Applied Biosystems, Waltham, MA, USA). Cycling conditions were as follows: initial denaturation, 95°C for 10 min; 40 cycles of denaturation (95°C for 15 s) and annealing (60°C for 1 min) with ramp rate of 1.6°C/s and a final melt curve step of 95°C for 15 s, 60°C for 1 min at 1.6°C/s and 95°C for 15 s with ramp rate of 0.05°C/s. Data acquisition and analyses were undertaken using the QuantStudio software version 1.3, including comparative CT (ΔΔCT) analyses. PCR product specificity was confirmed by melting curve analyses. Reverse transcriptase–negative complementary DNA samples and water were used in SYBR reactions as controls. Forward and reverse primer sequences for mouse and human primers are presented in Supplementary table 2.

Immunostaining, immunofluorescence and histology

Following formalin fixation and paraffin embedding, histological assessment of mouse stomachs and patient gastric biopsies were performed on 4–6-µm hematoxylin and eosin–stained tissue sections. Gastric mucosal thickness was measured as previously published.[18,31] Immunohistochemistry with primary antibodies against PCNA (ab18197; Abcam, Cambridge, UK), CD45 (550539; BD Biosciences, Franklin Lakes, NJ, USA), CD68 (ab125212; Abcam), CD3 (sc-1127; Santa Cruz, TX, USA), AIM2 (HPA031365; Atlas Antibodies, Stockholm, Sweden) and Ki67 (16 667; Abcam) was performed on gastric tissue sections as described previously.[28] For immunohistochemistry with a primary antibody against cleaved caspase-1 (PA5-105049; p10, cleaved caspase-1 Ala317; Invitrogen, Waltham, MA, USA) on formalin fixation and paraffin embedding tissue sections, antigen retrieval was performed with ethylenediaminetetraacetic acid buffer (1 mM, pH 8.0), using a 1–2-h block in CAS-Block (Thermo Fisher, Waltham, MA, USA). Sections were counterstained with hematoxylin. Immunofluorescence staining for cleaved caspase-3 (9661; Cell Signaling Technologies, Danvers, MA, USA), PCNA (ab18197; Abcam), E-cadherin (3195P; Cell Signaling Technologies) and CD45 (550 539; BD Biosciences) was performed as described previously.[24] Primary antibodies were detected with Alexa Fluor secondary antibodies and nuclear staining was performed with 4′,6-diamidino-2-phenylindole. Individual positively stained cells were counted manually in a blinded manner by investigators using ImageJ analysis software (National Institutes of Health, Bethesda, MD, USA). The number of positively stained cells was counted per high-power (×40) field, excluding areas containing lymphoid follicles, of 500 µm × 350 µm (immunohistochemistry) and 350 µm × 350 µm (immunofluorescence) (n = 5).

Immunoblotting

Total protein lysates (25 µg) from snap-frozen mouse tissues were prepared for immunoblotting with antibodies against mouse caspase-1 (p45/p20) (AG-20B-0042-C100; AdipoGen, San Diego, CA, USA) and mouse actin (A4700; Sigma-Aldrich), as described previously.[28] Blots were visualized using enhanced chemiluminescence for caspase-1 or IR Dye 800 (Li-COR Biosciences, Lincoln, NE, USA) for actin, and imaged with the Bio-Rad ChemiDoc or the Odyssey Infrared Imaging System (LI-COR). Densitometry analysis of bands was quantified using ImageJ software (n = 5).

ELISA

IL-1β ELISA was performed on mouse serum as per manufacturer's instructions (R&D Systems, Minneapolis, MN, USA). Mature IL-18 ELISA was performed as described previously.[24]

Statistical analyses

All statistical analyses were performed using GraphPad Prism V9 software. Statistical significance ($P < 0.05$) between the means of two groups was determined using Student's t-test or the Mann–Whitney U-test. Statistical significance between the means of multiple groups were determined using ordinary one-way ANOVA with *post hoc* multiple comparisons pairwise tests. All data are presented as the mean ± standard error of the mean from at least three technical replicates. The log-rank test was used to calculate the statistical significance of the difference in survival.

ACKNOWLEDGMENTS

We thank Veit Hornung (Ludwig-Maximilians-Universität München, Munich, Germany) for kindly providing *Aim2*$^{-/-}$

mice. Open access publishing facilitated by Monash University, as part of the Wiley - Monash University agreement via the Council of Australian University Librarians.

AUTHOR CONTRIBUTIONS

Ruby E Dawson: Data curation; formal analysis; writing – original draft; writing – review and editing. **Virginie Deswaerte:** Data curation; formal analysis. **Alison C West:** Data curation. **Ekimei Sun:** Data curation; formal analysis. **Georgie Wray-McCann:** Data curation. **Thaleia Livis:** Data curation. **Beena Kumar:** Formal analysis. **Emiliana Rodriguez:** Data curation. **Cem Gabay:** Formal analysis; resources; supervision. **Richard L Ferrero:** Resources; writing – review and editing. **Brendan J Jenkins:** Conceptualization; formal analysis; supervision; writing – original draft; writing – review and editing.

CONFLICT OF INTEREST

All authors have no conflicts of interest to declare.

FUNDING INFORMATION

This work was funded by a Peer Reviewed Cancer Research Program Idea Award (CA210128) from the United States Department of Defense (BJJ). This work was also supported by the Operational Infrastructure Support Program by the Victorian Government of Australia, and a Project Grant (APP1139371) from the National Health and Medical Research Council (NHMRC) of Australia (BJJ). BJJ and RLF were supported by NHMRC Senior Research Fellowships.

DATA AVAILABILITY STATEMENT

The data that support the findings of this study are available from the corresponding author upon reasonable request.

REFERENCES

1. Fox JG, Wang TC. Inflammation, atrophy, and gastric cancer. *J Clin Invest* 2007; **117**: 60–69.
2. Correa P, Piazuelo MB. *Helicobacter pylori* infection and gastric adenocarcinoma. *US Gastroenterol Hepatol Rev* 2011; **7**: 59–64.
3. Noto JM, Ferrero RL. *Helicobacter pylori*-induced gastric carcinogenesis. In: Jenkins BJ, ed. Research and Clinical Applications of Targeting Gastric Neoplasms. Cambridge, MA: Academic Press; 2021:91–118.
4. Zhang XY, Zhang PY, Aboul-Soud MA. From inflammation to gastric cancer: role of *Helicobacter pylori*. *Oncol Lett* 2017; **13**: 543–548.
5. Tshibangu-Kabamba E, Yamaoka Y. *Helicobacter pylori* infection and antibiotic resistance – from biology to clinical implications. *Nat Rev Gastroenterol Hepatol* 2021; **18**: 613–629.
6. Salama NR, Hartung ML, Muller A. Life in the human stomach: persistence strategies of the bacterial pathogen *Helicobacter pylori*. *Nat Rev Microbiol* 2013; **11**: 385–399.
7. Viala J, Chaput C, Boneca IG, *et al*. Nod1 responds to peptidoglycan delivered by the *Helicobacter pylori* cag pathogenicity Island. *Nat Immunol* 2004; **5**: 1166–1174.
8. Li X, Liu S, Luo J, *et al*. *Helicobacter pylori* induces IL-1β and IL-18 production in human monocytic cell line through activation of NLRP3 inflammasome via ROS signaling pathway. *Pathog Dis* 2015; **73**: ftu024.
9. Castano-Rodriguez N, Kaakoush NO, Mitchell HM. Pattern-recognition receptors and gastric cancer. *Front Immunol* 2014; **5**: 336.
10. Semper RP, Mejias-Luque R, Gross C, *et al*. *Helicobacter pylori*-induced IL-1β secretion in innate immune cells is regulated by the NLRP3 inflammasome and requires the cag pathogenicity Island. *J Immunol* 2014; **193**: 3566–3576.
11. Semper RP, Vieth M, Gerhard M, Mejias-Luque R. *Helicobacter pylori* exploits the NLRC4 inflammasome to dampen host defenses. *J Immunol* 2019; **203**: 2183–2193.
12. Márquez-Rodas I, Longo F, Rodriguez-Ruiz ME, *et al*. Intratumoral nanoplexed poly I:C BO-112 in combination with systemic anti-PD-1 for patients with anti-PD-1-refractory tumors. *Sci Transl Med* 2020; **12**: eabb0391.
13. Man SM, Jenkins BJ. Context-dependent functions of pattern recognition receptors in cancer. *Nat Rev Cancer* 2022; **22**: 397–413.
14. West AC, Jenkins BJ. Inflammatory and non-inflammatory roles for toll-like receptors in gastrointestinal cancer. *Curr Pharm Des* 2015; **21**: 2968–2977.
15. Smith SM, Moran AP, Duggan SP, *et al*. Tribbles 3: a novel regulator of TLR2-mediated signaling in response to *Helicobacter pylori* lipopolysaccharide. *J Immunol* 2011; **186**: 2462–2471.
16. Otani K, Tanigawa T, Watanabe T, *et al*. Toll-like receptor 9 signaling has anti-inflammatory effects on the early phase of *Helicobacter pylori*-induced gastritis. *Biochem Biophys Res Commun* 2012; **426**: 342–349.
17. Smith MF Jr, Mitchell A, Li G, *et al*. Toll-like receptor (TLR) 2 and TLR5, but not TLR4, are required for helicobacter pylori-induced NF-κB activation and chemokine expression by epithelial cells. *J Biol Chem* 2003; **278**: 32552–32560.
18. Tang K, McLeod L, Livis T, *et al*. Toll-like receptor 9 promotes initiation of gastric tumorigenesis by augmenting inflammation and cellular proliferation. *Cell Mol Gastroenterol Hepatol* 2022; **14**: 567–586.
19. Tye H, Kennedy CL, Najdovska M, *et al*. STAT3-driven upregulation of TLR2 promotes gastric tumorigenesis independent of tumor inflammation. *Cancer Cell* 2012; **22**: 466–478.
20. Allison CC, Kufer TA, Kremmer E, Kaparakis M, Ferrero RL. *Helicobacter pylori* induces MAPK phosphorylation and AP-1 activation via a NOD1-dependent mechanism. *J Immunol* 2009; **183**: 8099–8109.
21. Benoit BN, Kobayashi M, Kawakubo M, *et al*. Role of ASC in the mouse model of *Helicobacter pylori* infection. *J Histochem Cytochem* 2009; **57**: 327–338.

22. Tu S, Bhagat G, Cui G, *et al.* Overexpression of interleukin-1beta induces gastric inflammation and cancer and mobilizes myeloid-derived suppressor cells in mice. *Cancer Cell* 2008; **14**: 408–419.
23. Shigematsu Y, Niwa T, Rehnberg E, *et al.* Interleukin-1β induced by *Helicobacter pylori* infection enhances mouse gastric carcinogenesis. *Cancer Lett* 2013; **340**: 141–147.
24. Deswaerte V, Nguyen P, West A, *et al.* Jenkins, inflammasome adaptor ASC suppresses apoptosis of gastric cancer cells by an IL18-mediated inflammation-independent mechanism. *Cancer Res* 2018; **78**: 1293–1307.
25. Man SM, Zhu Q, Zhu L, *et al.* Critical role for the DNA sensor AIM2 in stem cell proliferation and cancer. *Cell* 2015; **162**: 45–58.
26. Sharma BR, Karki R, Kanneganti TD. Role of AIM2 inflammasome in inflammatory diseases, cancer and infection. *Eur J Immunol* 2019; **49**: 1998–2011.
27. Ratsimandresey RA, Indramohan M, Dorfleutner A, Stehlik C. The AIM2 inflammasome is a central regulator of intestinal homeostasis through the IL-18/IL-22/STAT3 pathway. *Cell Mol Immunol* 2017; **14**: 127–142.
28. Dawson RE, Deswaerte V, West AC, *et al.* STAT3-mediated upregulation of the AIM2 DNA sensor links innate immunity with cell migration to promote epithelial tumourigenesis. *Gut* 2022; **71**: 1515–1531.
29. El-Zaatari M, Bishu S, Zhang M, *et al.* Aim2-mediated/IFN-β-independent regulation of gastric metaplastic lesions via $CD8^+$ T cells. *JCI Insight* 2020; **5**: e94035.
30. Ferrero RL, Wilson JE, Sutton P. Mouse models of *Helicobacter*-induced gastric cancer: use of cocarcinogens. *Methods Mol Biol* 2012; **921**: 157–173.
31. Balic JJ, Saad MI, Dawson R, *et al.* Constitutive STAT3 serine phosphorylation promotes *Helicobacter*-mediated gastric disease. *Am J Pathol* 2020; **190**: 1256–1270.
32. Dooyema SDR, Noto JM, Wroblewski LE, *et al.* *Helicobacter pylori* actively suppresses innate immune nucleic acid receptors. *Gut Microbes* 2022; **14**: 2105102.
33. Song S, Peng P, Tang Z, *et al.* Decreased expression of STING predicts poor prognosis in patients with gastric cancer. *Sci Rep* 2017; **7**: 39858.
34. Chen L, Feng J, Wu S, *et al.* Decreased RIG-I expression is associated with poor prognosis and promotes cell invasion in human gastric cancer. *Cancer Cell Int* 2018; **18**: 144.
35. Wilson JE, Petrucelli AS, Chen L, *et al.* Inflammasome-independent role of AIM2 in suppressing colon tumorigenesis via DNA-PK and Akt. *Nat Med* 2015; **21**: 906–913.
36. Hu S, Peng L, Kwak YT, *et al.* The DNA sensor AIM2 maintains intestinal homeostasis via regulation of epithelial antimicrobial host defense. *Cell Rep* 2015; **13**: 1922–1936.
37. Koch S, Nusrat A. The life and death of epithelia during inflammation: lessons learned from the gut. *Annu Rev Pathol* 2012; **7**: 35–60.
38. Zhang S, Moss SF. Rodent models of *Helicobacter* infection, inflammation, and disease. *Methods Mol Biol* 2012; **921**: 89–98.
39. Hu GQ, Song PX, Li N, *et al.* AIM2 contributes to the maintenance of intestinal integrity via Akt and protects against salmonella mucosal infection. *Mucosal Immunol* 2016; **9**: 1330–1339.
40. Hornung V, Ablasser A, Charrel-Dennis M, *et al.* AIM2 recognizes cytosolic dsDNA and forms a caspase-1-activating inflammasome with ASC. *Nature* 2009; **458**: 514–518.
41. Rathinam VAK, Jiang Z, Waggoner SN, *et al.* The AIM2 inflammasome is essential for host defense against cytosolic bacteria and DNA viruses. *Nat Immunol* 2010; **11**: 395–402.
42. Jang AR, Kang MJ, Shin II, *et al.* Unveiling the crucial role of type IV secretion system and motility of *Helicobacter pylori* in IL-1β production via NLRP3 inflammasome activation in neutrophils. *Front Immunol* 2020; **11**: 1121.
43. Drexler SK, Bonsignore L, Masin M, *et al.* Tissue-specific opposing functions of the inflammasome adaptor ASC in the regulation of epithelial skin carcinogenesis. *Proc Natl Acad Sci USA* 2012; **109**: 18384–18389.
44. Allen IC, TeKippe EM, Woodford RM, *et al.* The NLRP3 inflammasome functions as a negative regulator of tumorigenesis during colitis-associated cancer. *J Exp Med* 2010; **207**: 1045–1056.
45. Hu B, Elinav E, Huber S, *et al.* Inflammation-induced tumorigenesis in the colon is regulated by caspase-1 and NLRC4. *Proc Natl Acad Sci USA* 2010; **107**: 21635–21640.
46. Tengesdal IW, Menon DR, Osborne DG, *et al.* Targeting tumor-derived NLRP3 reduces melanoma progression by limiting MDSCs expansion. *Proc Natl Acad Sci USA* 2021; **118**: e2000915118.
47. Kennedy CL, Najdovska M, Jones GW, *et al.* The molecular pathogenesis of STAT3-driven gastric tumourigenesis in mice is independent of IL-17. *J Pathol* 2011; **225**: 255–264.
48. Gantuya B, El-Serag HB, Matsumoto T, *et al.* Gastric microbiota in *Helicobacter pylori*-negative and -positive gastritis among high incidence of gastric cancer area. *Cancers (Basel)* 2019; **11**: 504.
49. Shiota S, Thrift AP, Green L, *et al.* Clinical manifestations of *Helicobacter pylori*-negative gastritis. *Clin Gastroenterol Hepatol* 2017; **15**: 1037–1046.e3.
50. Lee A, Fox JG, Otto G, Murphy J. A small animal model of human *Helicobacter pylori* active chronic gastritis. *Gastroenterology* 1990; **99**: 1315–1323.
51. Paster BJ, Lee A, Fox JG, *et al.* Phylogeny of *Helicobacter felis* sp. nov., *Helicobacter mustelae*, and related bacteria. *Int J Syst Bacteriol* 1991; **41**: 31–38.

SUPPORTING INFORMATION

Additional supporting information may be found online in the Supporting Information section at the end of the article.

The cytosolic DNA sensor AIM2 promotes *Helicobacter*-induced gastric pathology via the inflammasome

Ruby E Dawson, Virginie Deswaerte, Alison C West, Ekimei Sun, Georgie Wray-McCann, Thaleia Livis, Beena Kumar, Emiliana Rodriguez, Cem Gabay, Richard L Ferrero, Brendan J Jenkins

Inventory of Supplemental Information

Supplementary figure 1: Immune cell infiltrates in stomachs of WT and *Aim2*-deficient *H. felis*-infected mice.

Supplementary figure 2: Suppressed gastric pathology in *Aim2*-deficient *H. felis*-infected mice is independent of gender.

Supplementary figure 3: Co-localisation of proliferating PCNA-positive epithelial and immune cells in *H. felis*-infected mouse gastric tissues.

Supplementary figure 4: Reduced Caspase-1 activity in *Aim2*$^{-/-}$ *H. felis* mouse stomachs is independent of gender bias

Supplementary figure 5: Gene expression analysis of selected immune homing receptors in *H. felis*-infected mouse gastric tissues.

Supplementary table 1: Gastritis patient biopsies with indicated *Helicobacter pylori* status and score of inflammation severity.

Supplementary table 2 Primer sequences used for qPCR gene expression assays.

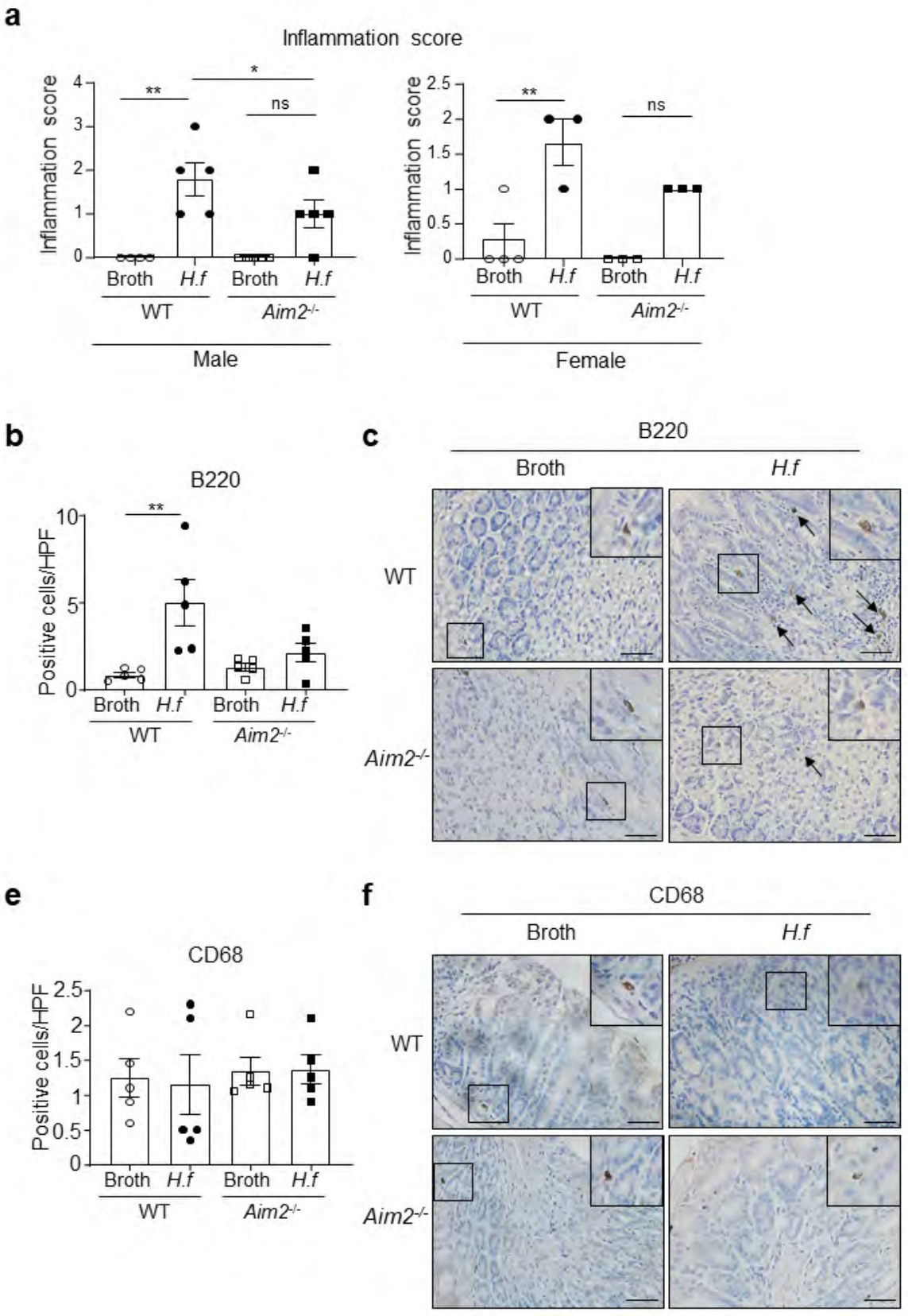

Supplementary figure 1: Immune cell infiltrates in stomachs of WT and *Aim2*-deficient *H. felis*-infected mice. (a) Gastric inflammatory scores (0–3; none, mild, moderate, severe) of

segregated male and female WT and *Aim2*$^{-/-}$ mice gavaged with *H. felis* or control broth (n = 3-5/group). **P* < 0.05, ***P* < 0.01; One-way ANOVA with multiple comparisons. ns, not significant. **(b)** Quantification of B220-positive stained cells in WT and *Aim2*$^{-/-}$ *H. felis* and broth gavaged mice (n = 5/group). ***P* < 0.01; One-way ANOVA with multiple comparisons. **(c)** Representative images of B220-positive immunostaining (arrows) in mouse gastric tissue cross-sections from WT and *Aim2*$^{-/-}$ *H. felis* and broth gavaged mice. Scale bars = 50μm. Insets at the top right of each image depict magnified areas (open squares) in the main images containing a B220-positive B cell. **(d)** Quantification of CD68-positive stained cells in WT and *Aim2*$^{-/-}$ *H. felis* and broth gavaged mice (n = 5/group). **(e)** Representative images of CD68 immunostaining in mouse gastric tissue cross-sections from WT and *Aim2*$^{-/-}$ *H. felis* and broth gavaged mice. Scale bars = 50μm. Insets at the top right of each image depict magnified areas (open squares) in the main images containing a CD68-positive macrophage.

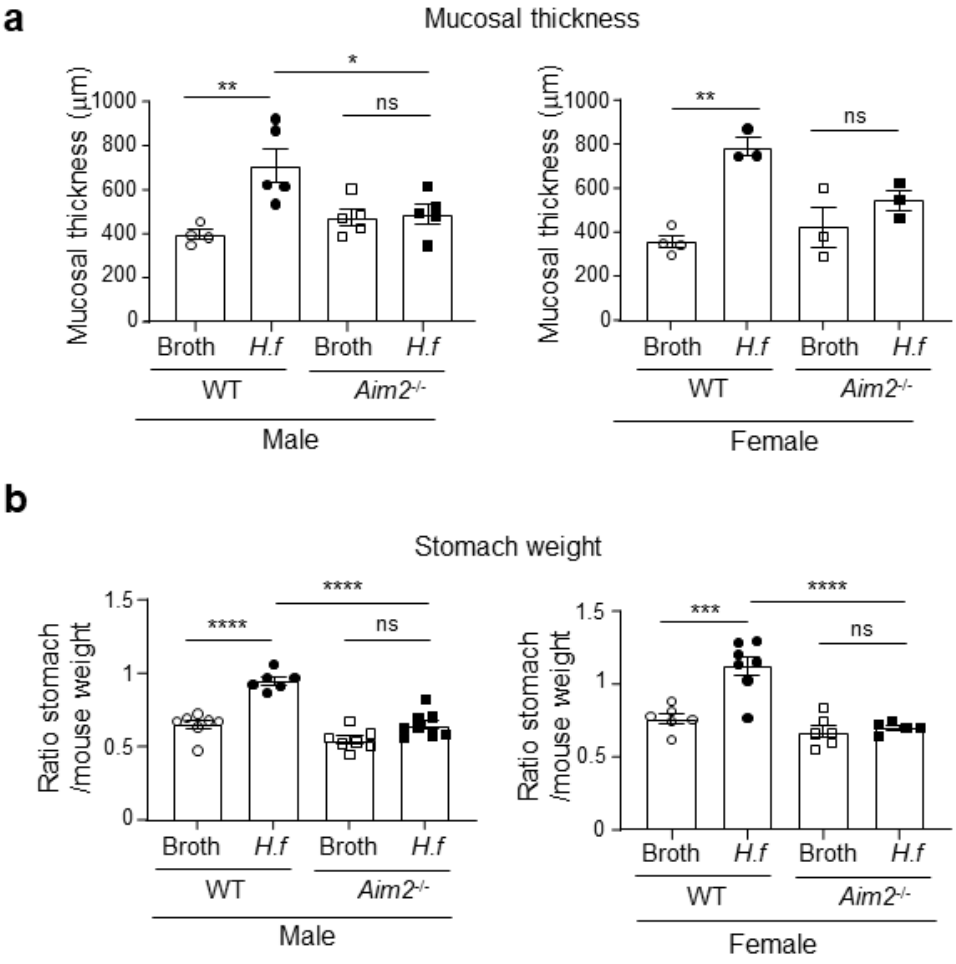

Supplementary figure 2: Suppressed gastric pathology in *Aim2*-deficient *H. felis*-infected mice is independent of gender. **(a)** Quantification of mucosal thickness of *H. felis* and control broth gavaged WT and *Aim2*$^{-/-}$ gastric corpus in mice segregated into males and females (n = 3-5/group). **P* < 0.05, ***P* < 0.01; One-way ANOVA with multiple comparisons. ns, not significant. **(b)** Ratio of stomach weight to total mouse weight for *H. felis* and control broth gavaged WT and *Aim2*$^{-/-}$ mice segregated into males and females (n = 5-8/group). ****P* < 0.001, *****P* < 0.0001; One-way ANOVA with multiple comparisons. ns, not significant.

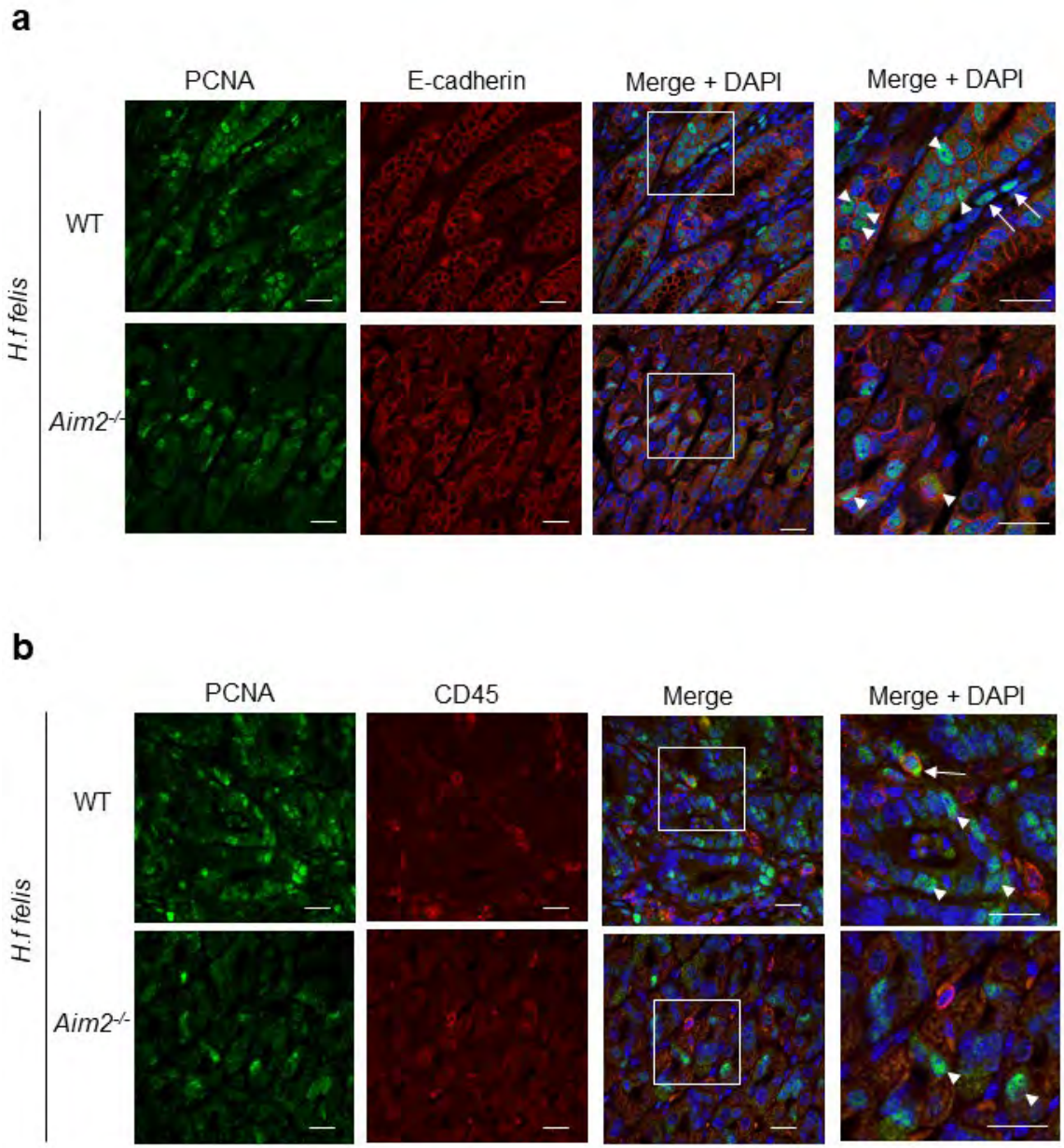

Supplementary figure 3: **Co-localisation of proliferating PCNA-positive epithelial and immune cells in *H. felis*-infected mouse gastric tissues.** Multicolour immunofluorescence staining for PCNA (green) and E-cadherin (red) **(a)**, and PCNA (green) and CD45 (red) **(b)**, in *H. felis* infected WT and *Aim2*$^{-/-}$ mouse gastric tissue cross-sections. In **(a)**, arrowheads indicate dual stained epithelial cells while arrows indicate E-cadherin negative, PCNA-only stained immune cells. In **(b)**, arrows indicate dual stained immune cells while arrowheads indicate CD45 negative, PCNA-only stained epithelial cells. Scale bars = 20μm.

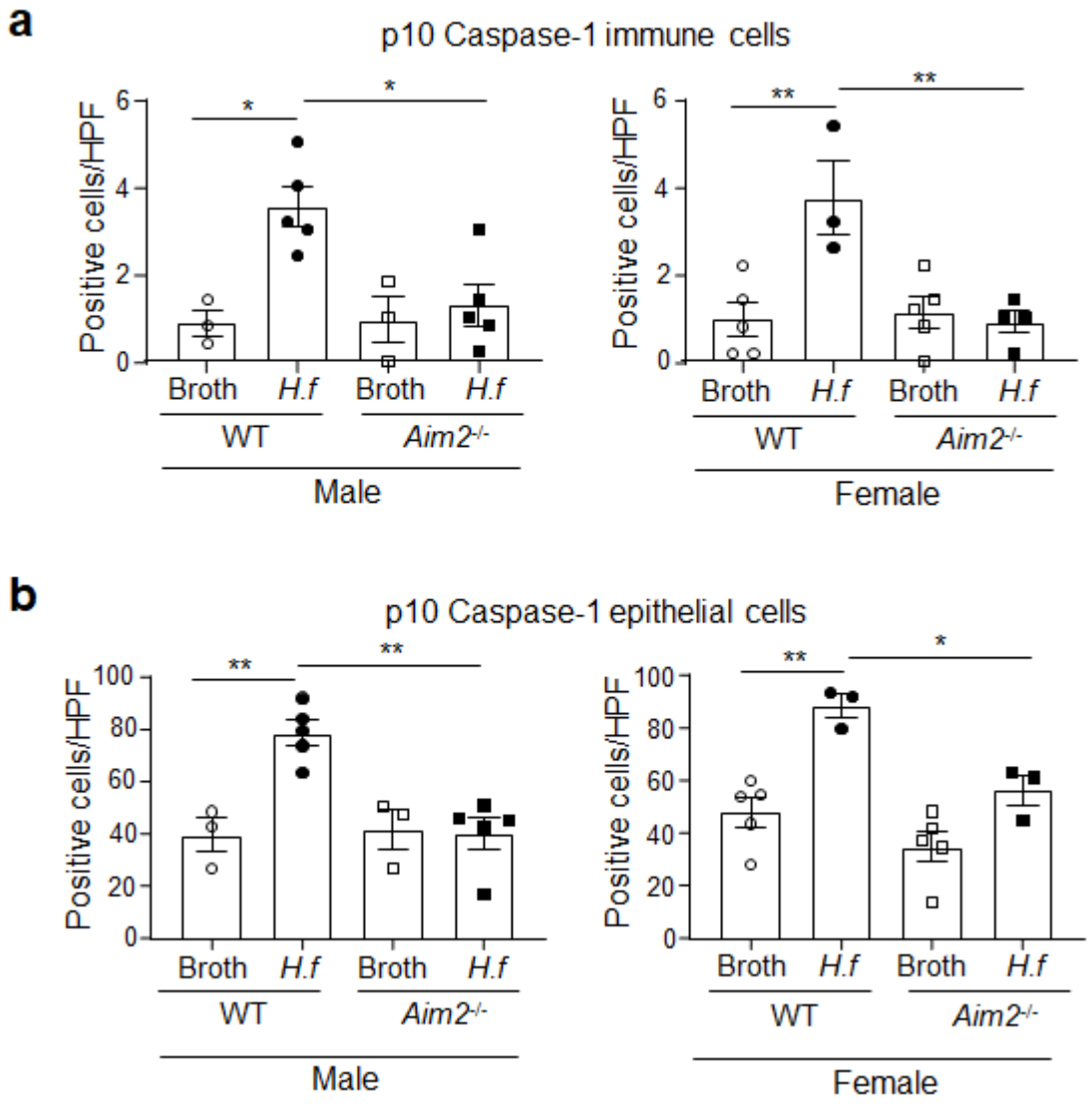

Supplementary figure 4: Reduced Caspase-1 activity in *Aim2*$^{-/-}$ *H. felis* mouse stomachs is independent of gender bias. (**a, b**) Graphs depict quantification of positively immunostained cleaved (p10) Caspase-1 **(a)** immune cells and **(b)** epithelial cells (from main Fig 6b) in gastric tissue sections from broth and *H. felis* gavaged WT and *Aim2*$^{-/-}$ mice that have been segregated into males and females (n = 3-5/group). **P* < 0.05, ***P* < 0.01; One-way ANOVA with multiple comparisons.

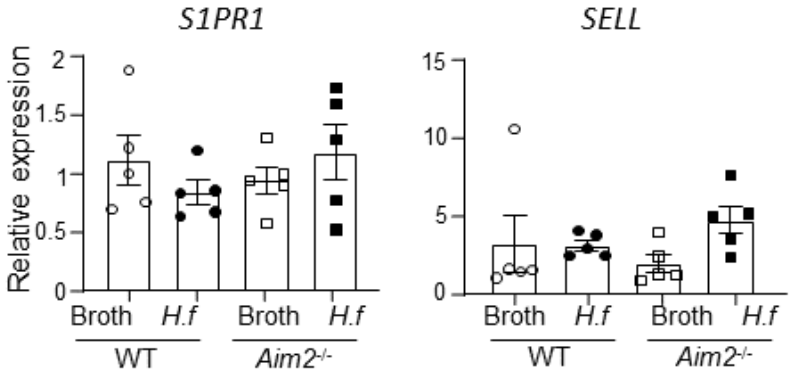

Supplementary figure 5: Gene expression analysis of selected immune homing receptors in *H. felis*-infected mouse gastric tissues. qPCR analysis for homing receptor genes in the indicated mouse gastric tissue samples (n = 5/group). Expression data are normalised to the *Rn18s* housekeeping gene.

Supplementary table 1: Gastritis patient biopsies with indicated *Helicobacter pylori* status and score of inflammation severity, N = normal, M = moderate, S = severe, Met = metaplasia. n.a = not available.

Patient ID	*Helicobacter* Status	Inflammation Status	Gender	Age
6	Negative	N	M	46
26	Negative	M/Met	F	60
45	Negative	N	F	56
50	Negative	N	n.a	n.a
63	Negative	N	M	67
67	Negative	M	n.a	n.a
55	Negative	M	n.a	n.a
52	Negative	N	n.a	n.a
9	Negative	M	M	71
16	Negative	M	F	74
29	Negative	S	n.a	n.a
32	Negative	M	F	57
3	Negative	N	M	67
14	Negative	S	F	53
31	Negative	M	M	45
18	Negative	S/Met	M	73
28	Negative	S	M	42
3	Negative	N	n.a	n.a
21	Positive	S/Met	F	59
12	Positive	S/Met	M	64
39	Positive	S/Met	F	68
54	Positive	S	M	34
25	Positive	S	n.a	n.a
68	Positive	M	F	63
37	Positive	M	M	48
46	Positive	M	M	72
22	Positive	S	M	49
41	Positive	S	M	70

61	Positive	S	F	51
43	Positive	S/Met	F	74
24	Positive	S	F	72

Supplementary table 2: Primer sequences used for qPCR gene expression assays.

Species	Primer Name	Primer Sequence
HUMAN		
	PYCARD Forward	5'- GCACTTTATAGACCAGCACCG - 3'
	PYCARD Reverse	5'- GGCTGGTGTGAAACTGAAGA -3'
	CASP1 Forward	5'- CTTCCTTTCCAGCTCCTCAGGCA -3'
	CASP1 Reverse	5'- CGTGTGCGGCTTGACTTGTCC -3'
Mouse		
	Sell Forward	5'-TGCAGAAACACAGTGTGGAGCA-3'
	Sell Reverse	5'- AGAAATGCCAGCCCCGAGA -3'
	S1pr1 Forward	5'- GCGCGGTGTAGACCCAGAGT-3'
	S1pr1 Reverse	5'- GAGGGCGAGGTTGAGTGAGC-3'
	Casp1 Forward	5'- ACGCCATGGCTGACAAGATCCTG -3'
	Casp1 Reverse	5'- GGTCCCGTGCCTTGTCCATAGC-3'